EXPERIMENTAL AND NUMERICAL STUDIES OF GRAIN SCALED BED-LOAD TRANSPORT

by

Jaeho Shim

A Dissertation Submitted to the Faculty of the

DEPARTMENT OF CIVIL ENGINEERING AND ENGINEERING MECHANICS

In Partial Fulfillment of the Requirements

For the Degree of

DOCTOR OF PHILOSOPHY

In the Graduate College

THE UNIVERSITY OF ARIZONA

2017

THE UNIVERSITY OF ARIZONA
GRADUATE COLLEGE

As members of the Dissertation Committee, we certify that we have read the dissertation prepared by Jaeho Shim, titled 'Experimental and Numerical Studies of Grain Scaled Bed-Load Transport' and recommend that it be accepted as fulfilling the dissertation requirement for the Degree of Doctor of Philosophy.

_____ Date: 12/20/2016
Jennifer G. Duan

_____ Date: 12/20/2016
Kevin E. Lansey

_____ Date: 12/20/2016
Juan B. Valdes

_____ Date: 12/20/2016
Donald C. Slack

Final approval and acceptance of this dissertation is contingent upon the candidate's submission of the final copies of the dissertation to the Graduate College.

I hereby certify that I have read this dissertation prepared under my direction and recommend that it be accepted as fulfilling the dissertation requirement.

_____ Date: 12/20/2016
Dissertation Director: Jennifer G. Duan

STATEMENT BY AUTHOR

This dissertation has been submitted in partial fulfillment of the requirements for an advanced degree at the University of Arizona and is deposited in the University Library to be made available to borrowers under rules of the Library.

Brief quotations from this dissertation are allowable without special permission, provided that an accurate acknowledgement of the source is made. Requests for permission for extended quotation from or reproduction of this manuscript in whole or in part may be granted by the head of the major department or the Dean of the Graduate College when in his or her judgment the proposed use of the material is in the interests of scholarship. In all other instances, however, permission must be obtained from the author.

SIGNED: Jaeho Shim

AKNOWLEDGEMENTS

I would like to express my gratitude to the many people who have contributed to this dissertation. First and foremost, I would like to thank my advisor Professor Jennifer Duan. Her guidance, support, encouragement and patience throughout this study have been invaluable in helping me complete this work. I would also like to thank my dissertation committee, Dr. Kevin Lansey, Dr. Juan Valdes, and Dr. Donald Slack for their help, valuable instruction and guidance.

I also want to thank my colleagues Chunshui Yu, Yang Bai, Khalid Asadi, Michael Potucek and Kang Zhou for all the help they offered in my study. Also, thank to Dr. Donghwi Jung, Dr. Hongki Jo, and Hwee Hwang. I have learned so much from them, and it is a pleasant experience to work with all of them.

Finally, but certainly not least, I would like to express my deepest love and thanks to my parents, Jihoon Shim and Wolsik Choo, and my brother Jaeyoung Shim who have always believed in me and continuously supported me all of my endeavors. Thanks for your love and encouragement.

TABLE OF CONTENTS

ABSTRACT 7
CHAPTER 1: INTRODUCTION 9
1.1 Research Background 9
1.2 Methodology 13
1.2.1 Experimental method 13
1.2.2 Numerical method 15
1.3 Format of Dissertation 17
CHAPTER 2: PRESENT STUDY 18
2.1 Experimental study of bed-load transport using particle motion tracking (Appendix A) 18
2.2 Experimental and theoretical study of bed-load particle velocity (Appendix B) 19
2.3 Simulation of dam-break flow induced scour around bridge pier (Appendix C) 20
REFERENCES 22
APPENDIX A - EXPERIMENTAL STUDY OF BED-LOAD TRANSPORT USING PARTICLE MOTION TRACKING 25
Abstract 26
1. Introduction 26
2. Experimental Setup 29
2.1 Flume setup 29
2.2 Hydraulic and sediment transport parameters and conditions 30
2.3 Camera system setup 32
3. Particle Motion Tracking 33
3.1 Image processing 33
3.2 Particle motion tracking algorithm 34
4. Experimental Results 36
4.1 Accuracy of particle tracking 36
4.2 Instantaneous particle velocity 36
4.3 Travel length and time 38
4.4 Averaged velocity of particles 41
5. Sediment Transport Rate 42
6. Conclusion 44
Notation 45
References 47
APPENDIX B - EXPERIMENTAL AND THEORETICAL STUDY OF BED LOAD PARTICLE VELOCITY 59
Abstract 60
1. Introduction 60

2. Theoretical Development 64
2.1 Mechanics of particle motion 64
2.2 Distribution Function of Particle Velocity 70
3. Laboratory Experiment 72
3.1 Experiment setup 72
3.2 Image processing 74
4. Verification of Theoretical Equations 75
4.1 Particle velocity 75
4.2 Two sample Kolmogorov-Smirnov test 76
4.3 Variation of particle velocity distribution with turbulence intensity 77
5. Conclusion 79
Acknowledgements 79
Nomenclature 80
References 82
APPENDIX C - SIMULATION OF DAM BREAK FLOW INDUCED SCOUR AROUND BRIDGE PIER USING SPH 93
Abstract 94
1. Introduction 95
2. Numerical Model 97
2.1 Smoothed Particle Hydrodynamics (SPH) method 97
2.2 Governing equation of the SPH method 99
3. Laboratory Experiment and Numerical Setup 101
3.1 Experiment setup 101
3.2 Numerical model setup 102
4. Experimental Observation and Simulation Results 103
4.1 Model validation 103
4.2 Bed surface elevation 103
4.3 Maximum scour depth evolution 105
5. Conclusion 106
References 108

ABSTRACT

Accurately calculating bed load transport rate has been a challenge in hydraulic engineering for decades. Bed load transport depends on the interaction between flow and sediment particles. Analyzing the characteristic of sediment particles motion and determining the velocity of sediment particles on a river bed is essential to quantify the transport rate. Therefore, this dissertation reports on the methods and results of a three-phased investigation to analyze the bed-load transport at the grain scale.

The first research phase focused on the experimental study of bed-load transport using particle motion tracking. A series of experiments were conducted in a flume to study bed-load transport. The motion of bed-load particles was captured by a series of images taken by a high-speed camera. A novel particle motion tracking method was developed to automatically detect all the moving particles and calculate the instantaneous particle velocities. The instantaneous bed load transport rate was calculated based on particle velocity and the volume of moving particles. To verify this method, bed load transport rate based on the image processing technique was compared to the manually measured ones as well as data from other experiments. Results showed that the new technique made it possible to quantify the spatial and temporal variations of bed load transport rate at the individual particle scale.

The second research study focused on the theoretical study of bed load particle velocity and its distribution. A theoretical equation was derived for calculating the particle velocity and distribution at the equilibrium transport state. It was found the mean particle velocity is a function of average bed shear stress, and the instantaneous velocity of a bed load particle is dependent on the instantaneous bed-shear stress. The PDFs of particle velocity and bed shear

stress both vary with the turbulence intensity. Results showed that the newly derived theoretical equation accurately predicted the average particle velocity. The PDF of particle velocity is a log-normal function at high Reynolds number, while it is close to an exponential distribution at low Reynolds number.

The third research study focused on the numerical investigation of bed-load transport at the grain scale. In detail, this study was carried out mainly on sediment transport around a bridge pier. Bridge scour is commonly calculated based on the steady flow assumption. In practice, the peak discharge of a 100-year event is used for calculating the bridge scour depth. This will overestimate the scour depth, especially in arid and semi-arid region where the typical storms are high-peak and short duration flash floods. Therefore, the numerical test for simulating sediment transport around a bridge pier in unsteady condition was conducted by using the Smooth Particle Hydrodynamics (SPH) model. The simulation obtained by the DualSPHysics showed the scour process around bride pier in dam break flow. The results showed the local scour depth is affected by the large sediment load accompanying the dam break flow. The maximum scour depth was reached quickly, but only lasted for a few seconds before being back-filled by sediment. The maximum scour depth occurring under unsteady flow is much smaller than the calculated value using peak-flow discharge. In other words, using the peak-flow discharge for designing can overestimate the maximum scour depth in comparison to the actual conditions under a flash flood or any unsteady hydrograph.

CHAPTER 1: INTRODUCTION

1.1 Research Background

Bed load transport rate is the amount of bed load particles transported along with flow on the bed surface. It can be quantitatively measured as the volume or the mass of bed load particles passing through a unit width of a cross section within a period of time. Theoretically, to determine bed load transport rate, one needs to measure the velocity of each bed load particle. Due to irregular shapes, non-uniform sizes, and the randomness of particle motion, each particle has a distinct velocity at a given time and space. In addition, it's well known the thickness of the bed load layer is more than one particle diameter, which means some moving particles are visible on the bed surface, and some are hidden underneath. Furthermore, the mode of bed load particle motion can be rolling, sliding, and saltation, which makes the measurements of particle velocity even more challenging. Up until now, no method is capable of measuring the velocity of each bed load particle. To calculate bed load transport rate, researchers often use the average velocity of all the moving particles, and assume that this average velocity is only dependent on particle size and flow properties. Its shape, irregularity, orientation to flow on the bed surface, and buried depth were assumed not to affect the average particle velocity. Researchers (Fernandez Luque and Van Beek 1976; Abbott and Francis 1977; Bridge and Dominic 1984; Van Rijn 1984; Wiberg and Smith 1985; Sekine and Kikkawa 1992; Lee and Hsu 1994; Niño and García 1994b; Niño and García 1998) measured the velocity of an individual particle by tracking its trajectory either on fixed or mobile bed, and this velocity was assumed as the approximation of the average particle velocity. Because the saltation motion has a relatively large step length, particle trajectories are

easier to identified in the images, researchers often derived the mean properties of saltation motion. For example, Fernandez Luque and Van Beek (1976) measured the mean number of moving particles per unit and the average length of individual particle steps on a mobile bed using a 16 frame rates camera. Abbott and Francis (1977) used a high speed camera to capture the images of a single particle motion over a fixed bed surface. Not only the average particle velocity, but also the average saltation length and height were obtained by averaging over the selected particles. Bridge and Dominic (1984) obtained the velocity of a single saltation particle using its trajectory, and also derived an equation for calculating the average particle velocity on a fixed rough bed. Van Rijn (1984) found the majority of bed load particles were transported as saltation motion, and then derived a single-step saltation particle model for bed load transport at low Reynolds number. Wiberg and Smith (1985) studied the mechanism of saltation particle processes, and proposed a numerical model for the motion of a single saltation particle using the impacting and rebounding physical mechanism. Sekine and Kikkawa (1992) found a single saltation particle's velocity is a function of friction velocity and sediment fall velocity. Lee and Hsu (1994) analyzed the continuous images of saltation for their trajectories and velocities, and developed a mathematical model to simulate motion of a single saltation particle. Niño and García (1994b) and Niño and García (1998) used a high speed camera to captured the number of saltating particles moving, and also applied a mathematical model to study the average saltation velocity and bed load transport rate. Using previous researches' data, some regression analyses for the motion of bed load particles have been done by Cheng and Emadzadeh (2014), and Julien and Bounvilay (2013).

Despite many benchmark studies using a single particle (Fernandez Luque and Van Beek

1976; Abbott and Francis 1977; Bridge and Dominic 1984; Sekine and Kikkawa 1992; Lee and Hsu 1994; Niño and García 1994a), one major concern is that neither an individual particle nor a group of manually selected particles can sufficiently represent the mean properties of all the moving particles on the mobile bed surface. It's obvious that the statistical properties of particle velocity can only be obtained from the measurements of all the moving particles. The high-speed camera can capture consecutive images of all the moving particles, and the moving distance between two consecutive images can be extracted (Papanicolaou et al. 1999; Lajeunesse et al. 2010; Houssais and Lajeunesse 2012). Lajeunesse et al. (2010) and Houssais and Lajeunesse (2012) used Particle Tracking Velocimetry (PTV) to investigate the average velocity, density, and transport rate of moving particles. Compared to previous methods in which a single or a few particles were measured on a fixed bed, it was found to be better representation of all the moving particles. To simplify the analysis, researches often account for a number of selected particles instead of all the moving particles in an image when calculating the average particle velocity. This treatment was adopted because it's difficult to identify and track each individual particle when processing thousands of images either manually or by commercial software (e.g., ImageJ). Consequently, researchers (Valyrakis et al. 2010; Furbish et al. 2012; Tregnaghi et al. 2012a; Ancey and Heyman 2014; Armanini et al. 2015) used selected particles from these images to study the properties of bed load particle motion. Furbish et al. (2012) applied an imaging technology (ImageJ) to measure bed-load particle transport, and derived a probabilistic formulation for particle velocity in turbulent flow. Tregnaghi et al. (2012a) noted that the fluctuation of fluid force, grain resistance, and geometrical configuration of the mobile bed surface are the key factors for determining particle velocity. Valyrakis et al. (2010) showed that

fluctuation of turbulence influences the characteristics of saltation and lift and drag forces acting on the particles fluctuate with respect to time. Armanini et al. (2015) presented a theoretical approach to evaluate sediment transport rate using the averaged particle velocity and a probability density function for the particle travel length. Ancey and Heyman (2014) also observed the randomness of moving particles in their experiment and applied a stochastic model describing particle motion using the frame work of birth-death Markov processes. Cheng and Emadzadeh (2014) summarized 14 formulas for calculating bed load particle velocity. Because of different datasets used for deriving these formulas, there is no consensus on the average bed load particle velocity, as well as the probability density function (PDF) function for its distribution.

This study aims to use the instantaneous velocities of all the moving particles to obtain the average and statistical properties of bed load particle velocity using a newly developed video image based Particle Tracking technique (VIPT). This technique is capable of tracking all of the moving sediment particles on a bed surface without pre-coloring or isolating particles, and automatically calculating particle geometric properties and particle velocities (Shim and Duan 2013; Shim and Duan 2015). Also, this study derived analytical formulas for mean particle velocity and its density distribution function by treating bed-shear stress as a stochastic variable. Laboratory experiments were conducted to verify the theoretically derived equations, and the captured images were processed using the VIPT software. In addition, numerical investigation of bed-load transport at the grain scale was conducted. In detail, this study was carried out mainly on local scour around a bridge pier in unsteady flow by using the Smooth Particle Hydrodynamics (SPH) model. The simulation obtained by the DualSPHysics showed the scour

process around the bridge pier in dam break flow. To calibrate and verify the model, the modelling results of particle velocities were compared with laboratory experimental results at the same condition. And then extended as a numerical flume to study bridge scour in high intensified dam break flow, which cannot be reproduced in the laboratory.

1.2 Methodology

The research focused on investigation of the bed-load particle motion and sediment transport in mobile bed channels at the grain scale and the study of a method for predicting the bed-load rate from particle motion tracking. To achieve this, experimental and numerical investigation were conducted. The experimental study was conducted to study the bed-load moving particles by using the newly developed particle motion tracking technique, and the numerical study applied the results from experimental studies to simulate bed-load particle transport at the grain scale.

1.2.1 Experimental method

The motion of sediment particles was captured by a high-speed digital camera (Sony XCD-V60). The camera can achieve up to 120 frames per second (fps) with a resolution of 640×480 pixels. This camera was mounted on a rod, and placed vertically just above the water surface. The rod was clamped to the flume so that they would incline together at the same angle. A small flat transparent plastic plate was placed on the water surface to remove image distortions caused by the light refraction from water-surface fluctuations. This placement ensures the camera has a clear view of the moving particles. To minimize the effects of pressurization caused by the local contraction surface, the plastic plate was very thin and could float freely right on the flow surface without imposing any force. Although the plastic plate doesn’t impose any pressure force, there

is minimal friction force on the water surface. The ratio of particle size to flow depth is from 3.7% to 8%. This minor friction effect was assumed to be negligible in this study, which needs to be noticed by other researchers interested in the data.

The camera was connected to and controlled by a computer, and automatically transferred captured images to the computer hard drive. Preliminary tests showed that the best image quality was achieved at a frame rate of 90 fps, suitable for capturing clear particle motion pictures. The minimum number of pixels for one sediment particle area is approximately 30, which is the threshold pixel size for determining the size and location of a particle. The test duration for each run was typically 16 seconds, but varied by the frame rate. In this study, over 1,300 consecutive images were captured during each run at the frame rate of 90 fps. To ensure the captured images are representative, 3-5 series of images were captured for each run. In the image analysis, if two or more series yielded the same results of particle velocity and deviation, one series was selected as the representation of the experimental run. If none of the series replicated the other, this run failed, and the data was not used.

A particle tracking algorithm was developed to track particles' trajectory Shim and Duan (2015) using the motion detection algorithm in OpenCV Library (http://code.opencv.org). At first, the captured digital picture images were converted to binary images for processing. Secondly, each moving particle was identified and isolated by a motion detecting algorithm based on image subtraction. This was performed by background subtraction between consecutive images to detect any moving particles in the frame. Thirdly, each image was processed by using morphological erosion and dilation transformations. This erosion and dilation process allows all the identified moving particles to have a distinct particle shape. After this process, a binary

image of a moving particle was obtained, and then the x- and y- coordinates of each particle were calculated as well.

Several criteria were applied to track a particles' trajectory. The first criterion is to use the particle size, which was compared with the original one in the searching area, through its particle size ratio. Another criterion is the color information within each particle. Using the origin image overlapped with the outline of moving particles, the histogram of color within each outline of a moving particle was extracted. The third criterion is to measure the minimal distance between the moving particles. These distinctive parameters of particles were used together to track the particle in the consecutive images. The best match is considered the location of the tracking particle. This image processing technique is capable of accurately detecting all the moving particles so that their instantaneous velocities can be calculated by comparing two consecutive images. These measurements were the database for calculating the statistical properties.

1.2.2 Numerical method

A three-dimensional hydrodynamic model is required to examine the fluid field around the bridge pier and the role of sediment transport in the scour process. Adequately resolving the interface is essential to capturing complex flows accurately with variable physical properties for each phase, such as free surface flows around bridge piers and impacting piers. Hence, a multi-phase SPH simulation needs both a huge number of particles and many time steps. Therefore, despite its suitability for such problems, SPH is well known for being an expensive method computationally (Crespo et al. 2011); and multi-phase SPH simulations naturally involve many more particles, further increasing the computational demands and costs (Mokos et al. 2015). In recent years, the massively parallel architecture of graphic processing units (GPUs) has emerged

as a viable option to process a large number of particles. The parallelization on GPUs makes them suitable for Lagrangian methods of SPH (Herault et al. 2010; Crespo et al. 2011). Accelerating SPH on a GPU is therefore the method of choice in this paper. Herein, we used the open source DualSPHysics code (Crespo et al. 2015) to include the two-phase liquid-solid model. DualSPHysics is a CPU/GPU solver package with pre- and post-processing tools capable of performing simulations on millions of particles using the GPU architecture targeted to practical engineering problems involving nonlinear, fragmented, and free-surface flows.

The multi-phase model in DualSPHysics code is applied to study a bam break flow induced scour around the bridge pier. In DualSPHysics, the experimental domain is discretized into a collection of particles with a particle size of 0.004 m. The numerical test case consists of a dam break problem confined within a rectangular box 2.0 m long, 0.45 m wide and 1.0 m high. The length of the numerical flume was reduced to minimize the number of SPH particles which allowed a reduction in the analysis time, however the circular pier was placed at the same location 1.4 m from the gate as the physical model. The volume of water initially contained behind a gate, and maximum water tank size is 0.3 m long, 0.45 m wide and 1.0 m high. As a result, the total number of particles is about 1.2million, of which 0.6 million are fluid particles, and 0.4 million are sediment particles. The remaining particles are boundary and gate particles. To ensure that the free surface is smooth and physically acceptable, the particle density is Shephard filtered every 20 steps (Dalrymple and Rogers 2006). Regarding the speed of sound C_s, it is chosen based on the principle that the ratio C_s/u_{max} should be larger than 10 (Monaghan 1994). The numerical simulations were carried out by running DualSPHysics on NVIDIA

GeForce 950 GPUs. The numerical model simulates 3 seconds of the physical experiment, and it requires approximately 40 *Hrs* of computation for cases with a bridge pier downstream.

1.3 Format of Dissertation

The research in this dissertation focused on the investigation of the bed-load particle motion and sediment transport in mobile bed channels at the grain scale and the study of a method for predicting the bed-load rate from particle motion tracking. The dissertation includes three different research studies and the format follows journal paper format. Three research manuscripts are reproduced in the Appendices.

CHAPTER 2: PRESENT STUDY

2.1 Experimental study of bed-load transport using particle motion tracking (Appendix A)

The purpose of this study was to apply a newly developed particle tracking method to accurately measure the velocities of all the moving bed load particles at various flow conditions. The study selected flow conditions and sediment particles where both rolling and saltating motion is present. This study developed a particle tracking method that can automatically identify moving particles, match them in consecutive images, and automatically compute particle velocity and bed load transport rate. This complete measurement of the particle velocity field enabled the study of bed load transport at the particle scale. Results showed that the particle tracking algorithm can automatically distinguish multiple moving particles in each frame and track the motion of each particle on a mobile bed surface. Using this result, high levels of accuracy were achieved for the measurement of bed load transport rate and particle velocity when saltating and rolling/sliding motions occur simultaneously. This data supplemented the data from Roseberry et al. (2012), Recking et al. (2008) at low shear stress, and evaluated the exponential-like PDFs for the streamwise and transverse particle velocities.

In addition, the travel length and time of all the moving particles were empirically correlated with flow shear velocity. The results indicate the travel length is nearly a constant at low shear velocity ($u_* / V_s < 0.25$), when sliding/rolling motion was dominant. However, when the shear velocity is greater than 0.25, the travel length increases rapidly. Bed-load transport rate measured by using the particle tracking method was compared with the manually measured ones.

The results confirmed that the particle tracking method presented in this paper made it possible to measure bed load transport rate at the individual particle scale, including the spatial and temporal variations of bed load transport rate. However, the experimental data was limited to uniform sized sediment with the particle Reynolds numbers ranging from 90 to 150. Also, the experimental data is only limited to particle transport at low shear stress. It is expected that this method will be applicable to flows with high sediment transport rate by using cameras with a sampling frequency of 200-500 Hz.

2.2 Experimental and theoretical study of bed-load particle velocity (Appendix B)

This study aims to use the instantaneous velocities of all the moving particles to obtain the average and statistical properties of bed load particle velocity. The experiments were performed in a rectangular channel filled with a layer of coarse sand or gravel. The instantaneous particle velocity was measured by using the images captured with a commercial camera. Both the mean particle velocity and the distribution of particle velocities were analyzed. Using this data, a theoretical equation was derived for calculating the particle velocity and distribution at the equilibrium transport state. It was found the mean particle velocity is a function of average bed shear stress, and the instantaneous velocity of a bed load particle is dependent on the instantaneous bed-shear stress. The PDFs of particle velocity and bed shear stress both vary with the turbulence intensity. To verify this, a series of laboratory experiments were performed, and particle velocity was measured using a new image-processing technique. The two sample Kolmogorov-Smirnov (K-S) test was conducted to examine the agreement between the

cumulative distributions of experimental data and distributions obtained from the theoretical model. Results showed that the newly derived theoretical equation accurately predicted the average particle velocity. The PDF of particle velocity is a log-normal function at high Reynolds number, while it is close to an exponential distribution at low Reynolds number.

2.3 Simulation of dam-break flow induced scour around bridge pier (Appendix C)

Bridge scour is commonly calculated with the steady flow assumption. In practice, the peak discharge of a 100-year event is used for calculating the bridge scour depth. However, the general practice of employing peak-flow discharge to evaluate the maximum scour depth for design may be questioned because the maximum scour depth occurring under flash floods can be much smaller than the calculated value using peak-flow discharge, especially in arid and semi-arid regions where the typical storms are high-peak and short duration. In other words, using the peak-flow discharge for design can overestimate the maximum scour depth in comparison to the actual conditions under the flash flood or any unsteady hydrograph.

Therefore, this research aims to measure the velocity of sediment particles, and get an insight of scour hole forming processes around bridge piers in unsteady flow. To get an insight of the scour process, scour monitoring is needed for a better understanding of the local scour process and to enhance the numerical models' capability of scour simulation. An experimental and numerical investigation of local scour around a bridge pier in dam break flow was conducted. A set of experiments were performed in a laboratory flume to produce dam break flow on a mobile bed with a pier installed downstream of the dam. The numerical simulation of

sediment transport around a bridge pier was conducted by using the Smooth Particle Hydrodynamics (SPH) model. The simulation obtained by the DualSPHysics showed the scour process around a bride pier in dam break flow. To calibrate and verify the model, the modelling results of particle velocities were comparted with laboratory experimental results under the same condition. Then it was extended as a numerical flume to study bridge scour in high intensified dam break flow, which cannot be reproduced in the laboratory. The results showed the local scour depth is affected by the large sediment load accompanying the dam break flow. The maximum scour depth was reached quickly, but only lasted for a few seconds before being back-filled by sediment. The ultimate scour depth is much smaller than the maximum scour depth. At present, the simulation domain is small, and the water tank height is short, due to the large number of particles need for the scour simulation. Therefore, further research on the numerical method and experimental study need to be investigated.

REFERENCES

Abbott, J. E., and Francis, J. R. D. (1977). "Saltation and suspension trajectories of solid grains in a water stream." *Philos. Trans. R. Soc. London Ser. A*, 284(1321), 225-254.

Ancey, C., and Heyman, J. (2014). "A microstructural approach to bed load transport: mean behaviour and fluctuations of particle transport rates." *J. Fluid Mech.*, 744, 129-168.

Armanini, A., Cavedon, V., and Righetti, M. (2015). "A probabilistic/deterministic approach for the prediction of the sediment transport rate." *Adv. Water Resour.*, 81, 10-18.

Bridge, J. S., and Dominic, D. F. (1984). "Bed load grain velocities and sediment transport rates." *Water Resour. Res.*, 20(4), 476-490.

Cheng, N. S., and Emadzadeh, A. (2014). "Average Velocity of Solitary Coarse Grain in Flows over Smooth and Rough Beds." *J. Hydraul. Eng.-ASCE*, 140(6).

Crespo, A. C., Dominguez, J. M., Barreiro, A., Gomez-Gesteira, M., and Rogers, B. D. (2011). "GPUs, a New Tool of Acceleration in CFD: Efficiency and Reliability on Smoothed Particle Hydrodynamics Methods." 6(6).

Crespo, A. J. C., Dominguez, J. M., Rogers, B. D., Gomez-Gesteira, M., Longshaw, S., Canelas, R., Vacondio, R., Barreiro, A., and Garcia-Feal, O. (2015). "DualSPHysics: Open-source parallel CFD solver based on Smoothed Particle Hydrodynamics (SPH)." 187, 204-216.

Dalrymple, R. A., and Rogers, B. D. (2006). "Numerical modeling of water waves with the SPH method." 53(2-3), 141-147.

Fernandez Luque, R., and Van Beek, R. (1976). "Erosion and transport of bed-load sediment." *J. Hydraul. Res.*, 14(2), 127-144.

Furbish, D. J., Haff, P. K., Roseberry, J. C., and Schmeeckle, M. W. (2012). "A probabilistic description of the bed load sediment flux: 1. Theory." *J Geophys Res-Earth*, 117, F03031.

Herault, A., Bilotta, G., and Dalrymple, R. A. (2010). "SPH on GPU with CUDA." 48, 74-79.

Houssais, M., and Lajeunesse, E. (2012). "Bedload transport of a bimodal sediment bed." *J. Geophys. Res.*, 117, F04015.

Julien, P. Y., and Bounvilay, B. (2013). "Velocity of rolling bed load particles." *J. Hydraul. Eng.*, 139(2), 177-186.

Lajeunesse, E., Malverti, L., and Charru, F. (2010). "Bed load transport in turbulent flow at the grain scale: Experiments and modeling." *J. Geophys. Res.*, 115, F04001.

Lee, H. Y., and Hsu, I. S. (1994). "Investigation of saltating particle motions." *J. Hydraul. Eng.*, 120(7), 831-845.

Mokos, A., Rogers, B. D., Stansby, P. K., and Dominguez, J. M. (2015). "Multi-phase SPH modelling of violent hydrodynamics on GPUs." 196, 304-316.

Monaghan, J. J. (1994). "Simulating free-surface flows with sph." 110(2), 399-406.

Niño, Y., and García, M., H. (1994a). "Gravel saltation 1. experiments." *Water Resour. Res.*, 30(6), 1907-1914.

Niño, Y., and García, M., H. (1994b). "Gravel saltation 2. modeling." *Water Resour. Res.*, 30(6), 1915-1924.

Niño, Y., and García, M., H. (1998). "Experiments on saltation of sand in water." *J. Hydraul. Eng.*, 124(10), 1014-1025.

Papanicolaou, A. N., Diplas, P., Balakrishnan, M., and Dancey, C. (1999). "Computer vision technique for tracking bed load movement." *J. Comput. Civil Eng.*, 13(2), 71-79.

Recking, A., Frey, P., Paquier, A., Belleudy, P., and Champagne, J. Y. (2008). "Bed-load transport flume experiments on steep slopes." *J. Hydraul. Eng.*, 134(9), 1302-1310.

Roseberry, J. C., Schmeeckle, M. W., and Furbish, D. J. (2012). "A probabilistic description of the bed load sediment flux: 2. Particle activity and motions." *J. Geophys. Res.*, 117, F03032.

Sekine, M., and Kikkawa, H. (1992). "Mechnics of saltating grains." *J. Hydraul. Eng.*, 118(4), 536-558.

Shim, J., and Duan, J. (2013). "Experiment study of bed load particle velocity." *Proc., World Environmental and Water Resources Congress 2013.* , Environ. Water Resour. Inst. American Soc. Civil Eng., 1962-1970.

Shim, J., and Duan, J. (2015). "Experimental study of bed-load transport using particle motion tracking." *Int. J. Sedi. Res.*, under review.

Tregnaghi, M., Bottacin-Busolin, A., Marion, A., and Tait, S. (2012a). "Stochastic determination of entrainment risk in uniformly sized sediment beds at low transport stages: 1. Theory." *J. Geophys. Res.-Earth Surf.*, 117, F04004.

Valyrakis, M., Diplas, P., Dancey, C. L., Greer, K., and Celik, A. O. (2010). "Role of instantaneous force magnitude and duration on particle entrainment." 115.

Van Rijn, L. C. (1984). "Sediment transport, part 1 : bed-Load transport." *J. Hydraul. Eng.*, 110(10), 1431-1456.

Wiberg, P. L., and Smith, J. D. (1985). "A theoretical model for saltating grains in water." *J. Geophys. Res.*, 90(C4), 7341-7354.

APPENDIX A - EXPERIMENTAL STUDY OF BED-LOAD TRANSPORT USING PARTICLE MOTION TRACKING

Jaeho Shim[1], Jennifer Duan[2]

Department of Civil Engineering and Engineering Mechanics, University of Arizona, Tucson, AZ 85721, USA

International Journal of Sediment Research

Abstract

A series of experiments were conducted in a flume to study bed-load transport. The motion of bed-load particles was captured by a series of images taken by a high-speed camera. A novel particle motion tracking method was developed to automatically detect all the moving particles and calculate the instantaneous particle velocities. The instantaneous bed load transport rate was calculated based on particle velocity and the volume of moving particles. To verify this method, bed load transport rate based on the image processing technique was compared to the manually measured ones as well as data from other experiments. Results showed that the new technique made it possible to quantify the spatial and temporal variations of bed load transport rate at the individual particle scale.

Keywords: Bed load transport; particle tracking; particle velocity

1. Introduction

Accurately calculating bed load transport rates has been a challenge in hydraulic engineering for decades. Bed load transport depends on the interaction between flow and sediment particles (Bridge & Dominic, 1984). Determining the velocity of sediment particles on a river bed is essential to quantify the transport rate. Many researchers (Bridge & Dominic, 1984; Francis, 1973; Lee & Hsu, 1994; Niño & García, 1994a; Novak & Nalluri, 1975; Sekine & Kikkawa, 1992) have studied the characteristics of particle motion and velocity. For example, images from high-speed cameras have enabled the accurate measurement of individual sediment motion (Francis, 1973; Furbish et al., 2012; Houssais & Lajeunesse, 2012; Lajeunesse et al., 2010; Lee

& Hsu, 1994; Niño & García, 1994b).

Advances in image processing techniques have permitted the continuous, multiple detections of moving particles, and also the automatic processing of captured images. For example, using consecutive images, fractional mobility of sediment particles was obtained by overlapping images of bed surface and identifying the sediments that remained immobile (Wu & Yang, 2004). Two particle motion tracking techniques, Eulerian (Radice et al., 2006) and Lagrangian frameworks (Heays et al., 2014; Houssais & Lajeunesse, 2012; Lajeunesse et al., 2010), are commonly used. Radice et al. (2006) used Eulerian framework, the Particle Image Velocimetry (PIV) technique, to measure the moving particle velocity. Eulerian technique is effective for detecting multiple moving particles. However, it is not suitable for tracking the motion of an individual particle. Lajeunesse et al. (2010) and Houssais and Lajeunesse (2012) used Lagrangian framework, Particle Tracking Velocimetry (PTV) to investigate the average velocity, density, and transport rate of moving particles. The PTV technique was also applied in a series of experiments using colored particles transported over fixed bed (Campagnol et al., 2013; Heays et al., 2014; Papanicolaou et al., 1999). However, due to large volumes of images, some researchers have chosen to analyze only the pre-colored particles, and others only selected representative images for manual processing.

Bed-load sediment moves along river bed by sliding, rolling, and saltating. Among them, saltating motion is dominant at high transport rate. Researchers (Bridge & Dominic, 1984; Fernandez Luque & Van Beek, 1976; Niño & García, 1994a) have used the trajectory of saltating particles to determine its velocity. These experiments were conducted either on fixed or mobile bed, and high-speed camera was employed to capture the images. Due to the limitation of the

camera and also the image processing technique, it's difficult to automatically distinguish and measure all the moving particles, so that only recognizable individual particle (e.g. saltating particles) was measured. From these limited experimental datasets, empirical equations of bed load transport were formulated primarily based on the measurements of saltating particles (Abbott & Francis, 1977; Bagnold, 1973; Francis, 1973; Lee & Hsu, 1994; Niño & García, 1994b). Because of this, rolling and sliding particles are often neglected, even though rolling particles can contribute significantly to bed load transport (Drake et al., 1988; Julien & Bounvilay, 2013). The number of moving particles in a given flow condition was not measured as well. Consequently, the resulting bed load transport equations are not an accurate representation of all the moving sediment. Recently, Papanicolaou et al. (2002) and Ramesh et al. (2011) investigated bed load transport having both rolling and saltation particles. Ramesh et al. (2011) also derived an empirical relation for rolling or saltating particles using the dimensionless flow and particle velocity parameters in Sekine and Kikkawa (1992). Tregnaghi et al. (2012a) found, at the incipient particle motion, the fluctuation of fluid force, grain resistance, and geometrical configuration of mobile bed surface are the key factors for determining particle velocity. However, those studies did not count all the moving particles, but only selected particles for image processing. Recent studies (Furbish et al., 2012; Roseberry et al., 2012) applied an imaging technology (ImageJ) to measure bed-load particle transport, and derived a probabilistic model for particle transport in turbulent flow. Their results showed that the distribution of particle velocity satisfies an exponential distribution. Ancey and Heyman (2014) applied a stochastic model to analyze bed load motions and concluded the fluctuations in the number of moving particles are Poisson at low shear stress, but depart from the Exner equation at

high shear stress. Conclusions from those studies regarding particle velocity and its statistical properties require additional independent verifications, and the correlations between particle transport properties and bed load transport rate also need to be explored further.

This study aims to apply a newly developed particle tracking method to accurately measure the velocities of all the moving bed load particles at various flow conditions. The study selected flow conditions and sediment particles where both rolling and saltating motions are present. The novel particle tracking method is capable of tracking all of the moving sediment particles on a bed surface without pre-coloring or isolating particles, and was programmed in C++ language using OPEN-CV library. This complete measurement of particle velocity field enables us to study bed load transport at the particle scale. Both the mean bed load transport rate, as well as the deviation of bed load transport rate were obtained from these measurements. These data supplemented the data from Roseberry et al. (2012), Recking et al. (2008) at low shear stress, and evaluated the exponential-like PDFs for the streamwise and transverse particle velocities. In the following sections, the experimental set-up, data processing technique, experimental result, and conclusion are presented in sequence.

2. Experimental Setup

2.1 Flume setup

The experiments were conducted in a rectangular titling flume, which is 0.15 m wide, and 2.4 m long. The side wall was made of Plexiglas, and its roughness is negligible compared to the roughness on a mobile bed surface. Bed slope was measured using a digital inclinometer with an accuracy of 0.1°. The incoming flow was pumped into the channel at constant discharges from a

large water tank, and controlled by a valve on the pipe. A honeycomb metal sheet was placed at the inlet to stabilize flow at the entrance. The measurement section is 0.12 m long, and located at 1.7 m away from the flume entrance. The bottom of the flume was covered by 5 cm deep uniformly sized sediment. This study used two groups of uniform sediment with median sizes of 1.5 mm and 2.4 mm, respectively (Table 1). The density of sediment is $\rho_s = 2650\ kg/m^3$. The standard deviations of sediment mixture, $\sigma_g = (d_{84}/d_{16})^{0.5}$, are 1.225 and 1.296, respectively. Sediment mixture with the value of σ_g less than 1.6 can be considered as uniform (Parker, 2008). During the experiment, sediment was fed into the flume externally at the entrance to ensure steady uniform flow condition. The feeding rate is approximately the transport rate we measured at the end of the flume. This is achieved by using all the sediment collected at the flume end. A total of 24 experimental runs were performed, and over 20,000 instantaneous particle velocities in the horizontal plane were measured. Those measurements were used to calculate the mean and standard deviation of particle velocities. A schematic experimental setup is shown in Fig. 1.

2.2 Hydraulic and sediment transport parameters and conditions

In each experiment, flow discharge was constant. There is a flat panel at the exit to regulate the water level. Without this panel, flow depth is critical at the exit. As the panel being raised slightly, a reach of uniform flow was observed in the flume. When water depths measured at five different locations along the flume were within 1 mm difference, the flow was treated as uniform. The streamwise bed shear stress, τ, is then approximated by

$$\tau = \rho g R S \tag{1}$$

where ρ is water density, g is the acceleration of gravity, R is hydraulic radius, and S is bed slope. The Shields number, τ_*, and the shear velocity are given by

$$\tau_* = \frac{\tau}{g(\rho_s - \rho)D} \tag{2}$$

$$u_* = \sqrt{\frac{\tau}{\rho}} = \sqrt{gRS} \tag{3}$$

where D is the size of sediment particle, and u_* is the friction velocity. Flow parameters and sediment characteristics for all the runs are summarized in Table 1. The critical shear stress was calculated as $\tau_c = \tau_{*c}(\gamma_s - \gamma)d_{50}$, in which γ_s, γ are the specific weight of sediment and water, respectively. A constant value of critical Shields number, $\tau_{*c} = 0.031$, for Re_* ranging from 90 to 150, was used in this study (Buffington & Montgomery, 1997). The thickness of viscous sublayer relative to that of the boundary roughness height determines if flow is hydraulic smooth, transitional, or rough (Le Roux, 2004). To distinguish different types of flow, the particle Reynolds number Re_* is calculated as:

$$\mathrm{Re}_* = u_* k_s / \nu \tag{4}$$

where k_s is the size of bed roughness, and ν is kinematic viscosity. When Re_* is less than 5, flow is smooth; and Re_* is greater than 60, it is rough. The transitional flow has Re_* between 5 and 60. In this study, the particle Reynolds number Re_* ranges from 90 to 150. Therefore, all the runs were conducted in the rough flow regime. For each run, the dimensionless bed load transport rate, Φ was calculated as:

$$\Phi = \frac{q_b}{\sqrt{(SG-1)gD^3}} \tag{5}$$

where q_b is bed load transport rate, $SG = \rho_s / \rho$, *is* the specific gravity.

2.3 Camera system setup

The motions of sediment particles were captured by a high-speed digital camera (Sony XCD-V60). The camera can achieve up to 120 frames per second (fps) with a resolution of 640×480 pixels. This camera was mounted on a rod, and placed vertically just above the water surface. The rod was clamped to the flume so that they would incline together at the same angle. A small flat transparent plastic plate was placed on the water surface to remove image distortions caused by the light refraction from water-surface fluctuations. This placement ensures the camera has a clear view of the moving particles. To minimize the effects of pressurization caused by local contraction surface, the plastic plate was very thin that can float freely right on the flow surface without imposing any force. Although the plastic plate doesn't impose any pressure force, there is minimal friction force on the water surface. The ratio of particle size to flow depth is from 3.7% to 8%. This minor friction effect was assumed to be negligible in this study, which needs to be noticed by other researchers interested in the data.

The camera was connected to and controlled by a computer, and automatically transferred captured images to the computer hard drive. Preliminary tests showed that the best image quality was achieved at a frame rate of 90 fps, suitable for capturing clear particle motion pictures. The minimum number of pixels for one sediment particle area is approximately 30, which is the threshold pixel size for determining the size and location of a particle. The test duration for each

run was typically 16 seconds, but varied by the frame rate. In this study, over 1,300 consecutive images were captured during each run at the frame rate of 90 fps. To ensure the captured images are representative, 3-5 series of images was captured for each run. In the image analysis, if two or more series yielded the same results of particle velocity and deviation, one series was selected as the representation of the experimental run. If none of the series replicated the other, this run failed, and the data was not used.

3. Particle Motion Tracking

This study developed a particle tracking method that is able to automatically identify moving particles, match them in consecutive images, and compute particle velocity and bed load transport rate. This automation of particle velocity measurements consists of three major steps: 1) detecting moving particles through background image subtraction, 2) transforming images using morphological processes, and 3) tracking particles by moving distance, contour area, and color histogram.

3.1 Image processing

The OpenCV library (http://code.opencv.org), a collection of computer graphics functions written in C++, was used for the image processing workflow programming. At first, the captured digital images were converted to binary images. Secondly, each image was subtracted from the background image taken when the bed was still. The remains from the subtraction are the particles being moved by flow (Bradski & Kaehler, 2008). Consequently, all the moving particles were isolated and identified in each image. Thirdly, morphologic erosion and dilation transformations were applied to identify each moving particle with a distinct shape. Erosion and

dilation are the most fundamental morphological transformation processes for removing noise, finding holes, isolating individual elements, and jointing disparate elements in the image. The erosion process removes the noise, such as very small motion of debris, and the dilation process was applied to fill some of the holes (e.g., empty pixels) inside the defined moving particles (Laganiere, 2011). As a consequence, a binary image having the edges of all the moving particles was obtained. The contour line (outline) of a moving particle is obtained by connecting the edge pixels of a particle. The locations of moving particles (x and y coordinates) were calculated as the geometric centers of those contours. Fourthly, the images having the contours of moving particles were then overlapped on the original image as shown in Fig. 2. This overlap recognizes the moving particles in the original image. The surface fraction of moving particles is then calculated as the fraction of the contour covered area in the image. Through those four processes, we obtained the location, size, and shape of all the moving particles in each image.

3.2 Particle motion tracking algorithm

To track particle's trajectory, some researchers used a minimal distance to find the best particle location (Campagnol et al., 2013; Frey, 2014), others used the similarity of surface area, the ratio between the surface area of a particle in two consecutive images, to locate the identical particle (Heays et al., 2014). In the present study, we applied several criteria to the subtracted images for tracking the particle. In the first image, each particle is tagged with a unique ID number. Then, a searching area (SA) for each particle was defined based on the maximum possible displacement in x- and y-directions, which is the product of the maximum flow velocity and the time interval between two images. The searching area has to be sufficiently large to encompass the trajectory of the fastest moving particle. In the consecutive image, if only one particle appeared in the SA,

this particle is the new location of the tagged particle. If more than one particle were identified in the SA, three criteria were used to search for the tagged one. The first criterion is to measure the distances between the tagged particle in the starting image and all the other particles in the consecutive image within the SA. The particle that has the minimum distance is the new location of the tagged particle. This criterion is suitable for tracking sparse moving particles at low bed load transport rate. Another criterion is to compare the ratios of surface area of each particle in the SA to that of the tagged particle. The particle having the ratio nearly equal to 1.0 is the new location of the tagged one. The third criterion is the color morphology within each particle contour. By overlapping the start and the consecutive images, the histograms of color values within the contour of the tagged particle and the captured ones in the SA were extracted. The tracking particle should have the best match of the color histogram with the tagged one. Those criteria were applied together to search for the tagged particle in the consecutive image. Ideally, all three search criteria need to be satisfied to confirm the new location of the tagged particle. In some cases, particularly, high transport rate, only two criteria were met for some particles.

Each particle has a unique ID number in the first image in which it appears. The same ID number was kept for the same particle in all the images allowing for the trajectory of each moving particle to be obtained by connecting the particle centers with the same ID number. The instantaneous particle velocity was calculated using the distance that the center of a particle had travelled in two consecutive images. According to the direction of particle motion, the total velocity was decomposed into the streamwise and transverse velocity. The entire image processing procedure was programmed by using the C++ language and OpenCV graphics library. The particle tracking algorithm was able to automatically distinguish multiple moving

particles and track the motion of each particle on mobile bed surface. This provided sufficient data for calculating the statistical properties of bed-load particle velocity and transport rate.

4. Experimental Results

4.1 Accuracy of particle tracking

In order to verify the accuracy of measured particle velocity and sediment transport rate using our particle tracking method, 100 consecutive images were processed, and the manually obtained particle velocity and sediment transport rate were compared with the computer processed ones. At first the number of moving particle in each image were manually counted, and then were matched with identical particles from different images. Results showed that the number of particles detected by the particle tracking algorithm is 93%. Some moving particles were missed because the particle were too small, or two particles were too close to separate in the automated procedure. The instantaneous velocities were also manually calculated using consecutive images. The distance travelled by one particle in two consecutive images was manually measured by a fine scaled ruler (1 mm accuracy). The instantaneous particle velocity, denoted by u_p, was calculated by dividing this distance by the time period between two frames. A velocity scale, $V_s = \sqrt{(SG-1)gD}$, is used to non-dimensionalize the instantaneous particle velocity. These manually calculated velocities were compared with those determined from the particle motion tracking in Fig. 3, where $u_{*p} = u_p / V_s$. Results from both methods matched very well.

4.2 Instantaneous particle velocity

The direction of particle motion was characterized by the orientation angle, θ, defined as

$\tan^{-1}(u_{yi}/u_{xi})$, where u_{xi} and u_{yi} are the i^{th} particle velocities in the streamwise and transverse directions, respectively. Fig. 4 is the frequency distribution of orientation angles, and shows that the direction of particle motion was nearly in the streamwise direction ($\tan\theta = 0$). In addition, the trajectories of several moving particles in ten successive images are illustrated in Fig. 5, where the arrows indicate the exact directions of moving particles. The time interval between two consecutive frames is 1/90 sec. It was noticed that the tracking algorithm successfully detected nearly all the moving particles including those having very minor displacements, typically less than the particle diameter. These particles of minor displacement are called the shaking particles that do not move down the channel, but re-adjust their positions according to the surrounding flow field. If the shaking particles are included, the spatially and temporally averaged particle velocity will be artificially reduced. To avoid this, a cutoff distance was set to exclude those particles for the velocity and transport rate calculation. The cutoff distance was about 0.4 – 0.7mm depending on the particle size and flow velocity.

Experimental research (Furbish et al., 2012; Furbish & Schmeeckle, 2013; Heays et al., 2014; Lajeunesse et al., 2010) has found that the probability density function (PDF) for the streamwise particle velocity is an exponential distribution, and that the PDF for the transverse particle velocity is a normal distribution with zero mean value, $\overline{u}_y = 0$. Experimental results from this study showed that the PDF of streamwise particle velocity are close to the exponential distribution (Fig. 6) as observed in Lajeunesse et al. (2010) and Roseberry et al. (2012). The probability density function is written as:

$$f(u_x) = \frac{1}{\overline{u}_x} e^{-u_x/\overline{u}_x} \tag{6}$$

where $\overline{u}_x$ is the average streamwise particle velocity. Eq. 6 slightly underestimated the experimental data at high particle velocity as shown in Fig.6. However, it's the best fitting curve we can find to match the observed data. This also confirms similar results from other researches (Furbish et al., 2012; Lajeunesse et al., 2010; Roseberry et al., 2012). The PDF of the transverse particle velocity is approximated by the Gaussian distribution as shown in Fig. 7.

$$f(u_y) = \frac{1}{\sigma\sqrt{2\pi}} e^{-((u_y - \overline{u}_y)/2\sigma)^2} \tag{7}$$

where σ is the standard deviation of transverse particle velocity, and $\overline{u}_y$ is the average transverse particle velocity. Although the Gaussian distribution matched the peak values very well, it underestimated the measurements at both tails.

4.3 Travel length and time

For each run, we measured all of the moving particles trajectories, including sliding, rolling, and saltating ones, with our particle tracking program. From those trajectories, we measured the travel length and time of all the moving particles. In Fig. 8, we plot the correlation between average L/D and u_*/V_s (the middle line). At low shear velocity ($u_*/V_s < 0.25$) the particle travel length is approximately a constant, 4.0. However, when the non-dimensional shear velocity is greater than 0.25, the travel length increases rapidly with the shear stress. This means when sliding/rolling motion is dominant at low shear velocity, the average particle travel length is about four times the particle size. As the shear stress increases, the saltating motion becomes dominant, and the particle travel length increases with the shearing stress shown in Fig.8 (the middle line). The empirical relations for the particle travel length are formulated as:

$$L/D \approx 4 \qquad u_*/V_s < 0.25 \qquad (8)$$

$$L/D = 32.2(u_*/V_s) - 4.5792 \qquad u_*/V_s \geq 0.25 \qquad (9)$$

It is known the travel length and time of a saltation motion is much greater than those of a sliding/rolling one. To separate the saltation motion from the sliding/rolling motions, the minimum distance of saltation motion and the maximum distance of sliding/rolling motions need to be defined. The experimental data showed two distinct regions of particle travel distance: one is above 7D, and the other is less than 3D. Over 80% of particles are resided in those two regions. Therefore, it is assumed a saltating motion travels at least 7D continuously, while a rolling/sliding motion travels less than 3D in a continuous motion. This differentiation of the saltating and rolling/sliding motion using the travel length is similar to those (Lee & Hsu, 1994; Niño & García, 1998) observed, but requires further laboratory verification. Based on this, the travel length and time for the saltation and rolling/sliding motions were calculated. The ratio of an identical particle surface area in two consecutive images is defined as A_i^n / A_i^{n+1}, where *i* is particle ID, and *n* is n^{th} of frame, is between 0.5 and 1.5. Then, it's considered as a saltating motion. Travel lengths for sliding/rolling and saltation particles, L/D, were constants, 2 and 8, respectively, when $u_*/V_s < 0.25$. When $u_*/V_s \geq 0.25$, the travel length linearly increased with the shear velocity. However, the linear relations for saltation and rolling/sliding motions are different. The empirical formulated equations are listed below:

For the saltating particles (Fig. 8 – the upper line):

$$L/D \approx 8 \qquad u_*/V_s < 0.25 \qquad (10)$$

$$L/D = 60.967(u_*/V_s) - 7.563 \qquad u_*/V_s \geq 0.25 \qquad (11)$$

For the sliding/rolling particles (Fig. 8 – the lower line):

$$L/D \approx 2 \qquad u_*/V_s < 0.25 \qquad (12)$$

$$L/D = 5.3848(u_*/V_s) + 0.4182 \qquad u_*/V_s \geq 0.25 \qquad (13)$$

In addition, the probability density function (PDF) of the travel lengths for all the moving particles, the sliding/rolling ones, and the saltating ones were plotted in Fig. 9a, 9b, 9c, respectively. Experimental results showed that the PDFs for the travel length (*L/D*) of both the saltating and sliding/rolling particles satisfie the Gamma distribution.

$$P(L/D) = \frac{L/D^{\alpha}}{\Gamma(\alpha+1)\beta^{\alpha+1}} e^{-\left(\frac{L}{D}\right)/\beta} \qquad (14)$$

where α and β are the shape and scale parameters with $\alpha>0$ and $\beta>0$, and Γ is the gamma function. In Fig. 9, for the PDF of saltating and rolling/sliding particles, the peak value of saltating travel length is about 10D, while the peak value for sliding/rolling particles is much less, about 2D.

The mean travel time, $\overline{T}$, normalized by the characteristic settling time as $T_* = \overline{T}/\sqrt{D/Rg}$, is shown in Fig. 10. The averaged dimensionless travel time, T_*, is nearly a constant for all the particles (Eq. 15), with saltating particles traveling about twice as long as those with shorten travel distances (Eq.16). Eq.17 is the dimensionless travel time for the rolling/sliding particles.

$$\overline{T}/\sqrt{D/Rg} = 4.8 \pm 0.6 \qquad \text{All of particle} \qquad (15)$$

$$\overline{T}/\sqrt{D/Rg} = 10.6 \pm 1.0 \qquad \text{Saltating particle} \qquad (16)$$

$$\overline{T}/\sqrt{D/Rg} = 2.43 \pm 0.25 \qquad \text{Rolling particle} \qquad (17)$$

4.4 Averaged velocity of particles

In addition to the instantaneous velocity measured using two consecutive images, the averaged velocity of all the moving particles were also calculated. Those velocities were calculated by dividing the travel distance of each particle in a continuous motion by the travel time. The average particle velocity is the average of all the velocities of moving particles at a given flow condition, which is plotted versus the friction velocity in Fig. 11. When u_*/V_s is smaller than 0.25, $\overline{u}_p/V_s$ ranges from 0.78 to 0.85, but when u_*/V_s is larger than 0.25, it increases linearly with u_*/V_s.

The velocity measurements were also compared with data from previous studies. Two different trends are visible depending on the nature of bed surface and the mode of particle motion. For a single particle above a fixed bed (Abbott & Francis, 1977; Lee & Hsu, 1994) or selective particle motions above an erodible bed (Fernandez Luque & Van Beek, 1976), the particle velocities were larger than those obtained by averaging over all measurements on mobile bed. It's apparent that a single or a few selected particles are not sufficient to represent the particle velocity over a mobile bed in this study. The interactions between particles impose a resistance force to decelerate the moving particles. Furthermore, as sediment particles are transported as a group on a mobile bed surface, the particle velocities are varying with particle sizes, shapes, and placements. When all the moving particles are taken into account, the averaged particle velocity should be smaller than those using a single or a few selected particles. Lajeunesse et al. (2010) also conducted experiments to record the velocities of all the moving

particles, and found a similar linear relation, but slightly smaller values than those in the present study for $u_*/V_s < 0.25$. This may be attributed to the fact that the study by Lajeunesse et al. (2010) used a larger sized particle.

5. Sediment Transport Rate

Bed load sediment transport rate is the sum of the product of each transported particle's volume and its velocity in the streamwise direction. The diameter of each particle is approximated by the equivalent diameter for the area enclosed by its contour, in which $D_i = \sqrt{4A_i/\pi}$, where A_i is the area of the i^{th} contour. The volume of a particle can be calculated as:

$$\forall_i = \frac{1}{6}\pi D_i^3 \tag{18}$$

where $\forall_i$ is the volume of the i^{th} particle at each frame. Sediment transport rate in mass per unit width and time is given by

$$q_{bj} = \frac{\sum_{i=1}^{n} \rho_s \forall_i u_{pi}}{A_s} \tag{19}$$

$$q_b = \frac{1}{N}\sum_{j=1}^{N} q_{bj} \tag{20}$$

where q_{bj} is the instantaneous bed load transport rate at the j^{th} frame, n is the total number of particle moving in j^{th} frame; N is the number of total frames; ρ_s is the density of sediment, u_{pi} is the instantaneous particle velocity for i^{th} particle, A_s is the area covered in the image, and q_b is the averaged bed-load transport rate over N frames. The physical samples of bed-load sediment were collected in 20-gallon basket at the end of the flume for 1.0 minute during each run to

verify the accuracy of the image-based calculations. Physically measured bed load transport rate was determined using the weight of sediment per unit time per unit width of the flume. A total of 29 bed load measurements were obtained. The bed load transport rates calculated by Eq. (21) were compared with the manually measured ones, as shown in Fig. 12. The results indicated that the mean error of Eq. (21) for calculating bed load transport rate is 5%. This result implies that the particle tracking method developed in this study is capable of measuring all the moving particles' velocities accurately regardless of sliding, rolling, or saltation motions.

Bed-load transport rate, calculated using the particle tracking method is presented in Fig. 13 along with data from previous researches (Recking et al., 2008; Roseberry et al., 2012) . Each transport rate from this study was calculated using 1,398 images obtained in 16 seconds. The dimensionless bed load transport rate is defined in Eq. 5. Three empirical sediment transport formulas were also plotted: the Meyer-Peter Muller formula (Meyer-Peter & Muller, 1948) $\Phi = 8(\tau_* - 0.047)^{3/2}$, the Fernandez Luque and Van Beek formula (Fernandez Luque & Van Beek, 1976) $\Phi = 5.7(\tau_* - 0.06)^{3/2}$, and Bohm formula (Bohm et al., 2006) $\Phi = 2(\tau_* - 0.056)^{3/2}$. The measured bed load transport rate using the particle tracking technique in this study were within the range of all three bed load transport equations. The match of our experimental results with these three formulas, as well as experimental and field data indicates that the particle tracking method will potentially enable the image based automation of bed load transport measurement. However, experimental data from this study have low shear stress. Additional data of particle velocity at high transport rate are needed to further verify this particle tracking method.

6. Conclusion

This study developed a particle tracking method that is able to automatically identify moving particles, match them in consecutive images, and automatically compute particle velocity and bed load transport rate. Results showed that our particle tracking algorithm can automatically distinguish multiple moving particles in each frame and track the motion of each particle on a mobile bed surface. Using this result, high levels of accuracy were achieved for the measurement of bed load transport rate and particle velocity when saltating and rolling/sliding motions occur simultaneously.

In addition, the travel length and time of all the moving particles were empirically correlated with flow shear velocity. The results indicate the travel length is nearly a constant at low shear velocity ($u_* / V_s < 0.25$), when sliding/rolling motion was dominant. However, when the shear velocity is greater than 0.25, the travel length increases rapidly. Bed-load transport rate measured by using the particle tracking method was compared with the manually measured ones. The results confirmed that the particle tracking method presented in this paper made it possible to measure bed load transport rate at the individual particle scale, including the spatial and temporal variations of bed load transport rate. However, the experimental data was limited to uniform sized sediment with the particle Reynolds numbers ranging from 90 to 150. And our experimental data are only limited to particle transport at low shear stress, we expect that this method will be applicable to flows with high sediment transport rate by using cameras with a sampling frequency of 200-500 Hz. Our ultimate goal is to apply this particle tracking method to natural rivers. In the future, we will collect field data using this technique to further verify its applicability.

Notation

A_i^n = area of the i^{th} contour (m^2);

A_s = surface area covered in the image (m^2)

D = diameter of sediment particle (m)

D_i = diameter of i^{th} sediment particle (m);

d_{16}, d_{50}, d_{84} = grain diameter for which 16%, 50% and 84 % are finer, respectively (m);

g = acceleration of gravity (ms^{-2})

k_s = size of bed roughness (m)

L = particle moving length (m)

N = number of total frames.

n = number of moving particles in the frame

q_b = bed-load transport rate per unit width ($\text{kg m}^{-1}\text{s}^{-1}$);

q_{bn} = sediment transport rate per unit width at the n^{th} frame ($\text{kg m}^{-1}\text{s}^{-1}$);

R = hydraulic radius (m);

Re_* = particle Reynolds number (–);

S = bed slope (–);

SG = specific gravity (–);

T_* = dimensionless travel time (–);

$\overline{T}$ = mean travel time (s);

u_p , u_x , u_y = instantaneous, streamwise and transverse particle velocity (ms^{-1});

u_{pi}, u_{xi}, u_{yi} = instantaneous, streamwise and transverse velocity of i^{th} particle (ms^{-1});

$\overline{u}_p$, $\overline{u}_x$, $\overline{u}_y$ = time-averaged particle velocity, and its components in streamwise and transverse directions, respectively (ms^{-1});

u_* = shear velocity (ms^{-1});

u_{*_p} = dimensionless instantaneous particle velocity (–)

V_s = reference velocity (ms^{-1})

w = width of test area (m);

α, β = shape and scale parameter, respectively;

γ, γ_s = specific weight of water and sediment, respectively(Nm^{-3});

θ = orientation angle of particle motion ($^\circ$)

ν = kinematic viscosity of water (m^2s^{-1})

ρ, ρ_s = density of water and sediment, respectively (kg m^{-3});

σ = standard deviation of particle velocity (ms^{-1});

σ_g = standard deviation of sediment particle size (m);

τ = bed shear stress (Nm^{-2});

τ_c = critical bed shear stress (Nm^{-2});

τ_* = Shields number of sediment particle (–);

τ_{*_c} = critical Shields number of sediment particle (–);

Φ = dimensionless sediment transport rate (–);

$\forall_i$ = volume of the i^{th} particle at each frame (m^3);

References

Abbott, J. E., & Francis, J. R. D. (1977). Saltation and suspension trajectories of solid grains in a water stream. *Philosophical Transactions of the Royal Society of London. Series A, 284*(1321), 225-254.

Ancey, C., & Heyman, J. (2014). A microstructural approach to bed load transport: mean behaviour and fluctuations of particle transport rates. *Journal of Fluid Mechanics, 744*, 129-168. doi: 10.1017/jfm.2014.74

Bagnold, R. A. (1973). Nature of saltation and of bed-load transport in water. *Proceedings of the Royal Society of London. Series A, 332*(1591), 473-504. doi: DOI 10.1098/rspa.1973.0038

Bohm, T., Frey, P., Ducottet, C., Ancey, C., Jodeau, M., & Reboud, J. L. (2006). Two-dimensional motion of a set of particles in a free surface flow with image processing. *Experiments in Fluids, 41*(1), 1-11. doi: 10.1007/s00348-006-0134-9

Bradski, G., & Kaehler, A. (2008). *Learning OpenCV* (M. Loukides Ed. 1st ed.). Sebastopol, CA: O'Reilly.

Bridge, J. S., & Dominic, D. F. (1984). Bed load grain velocities and sediment transport rates. *Water Resources Research, 20*(4), 476-490. doi: 10.1029/Wr020i004p00476

Buffington, J. M., & Montgomery, D. R. (1997). A systematic analysis of eight decades of incipient motion studies, with special reference to gravel-bedded rivers. *Water Resources Research, 33*(8), 1993-2029. doi: 10.1029/96wr03190

Campagnol, J., Radice, A., Nokes, R., Bulankina, V., Lescova, A., & Ballio, F. (2013). Lagrangian analysis of bed-load sediment motion: database contribution. *Journal of Hydraulic Engineering, 51*(5), 589-596. doi: 10.1080/00221686.2013.812152

Drake, T. G., Shreve, R. L., Dietrich, W. E., Whiting, P. J., & Leopold, L. B. (1988). Bedload transport of fine gravel observed by motion-picture photography. *Journal of Fluid Mechanics, 192*, 193-217. doi: 10.1017/s0022112088001831

Fernandez Luque, R., & Van Beek, R. (1976). Erosion and transport of bed-load sediment. *Journal of Hydraulic Research, 14*(2), 127-144. doi: 10.1080/00221687609499677

Francis, J. R. D. (1973). Experiments on the motion of solitary grains along the bed of a water-stream. *Proceedings of the Royal Society of London. Series A, 332*(1591), 443-471.

Frey, P. (2014). Particle velocity and concentration profiles in bedload experiments on a steep slope. *Earth Surface Processes and Landforms, 39*(5), 646-655. doi: 10.1002/esp.3517

Furbish, D. J., Roseberry, J. C., & Schmeeckle, M. W. (2012). A probabilistic description of the bed load sediment flux: 3. The particle velocity distribution and the diffusive flux. *Journal of Geophysical Research-Earth Surface, 117*, F03033. doi: 10.1029/2012jf002355

Furbish, D. J., & Schmeeckle, M. W. (2013). A probabilistic derivation of the exponential-like distribution of bed load particle velocities. *Water Resources Research, 49*(3), 1537-1551. doi: 10.1002/wrcr.20074

Heays, K. G., Friedrich, H., Melville, B. W., & Nokes, R. (2014). Quantifying the dynamic evolution of graded gravel beds using particle tracking velocimetry. *Journal of Hydraulic Engineering, 140*(7), 04014027. doi: 10.1061/(asce)hy.1943-7900.0000850

Houssais, M., & Lajeunesse, E. (2012). Bedload transport of a bimodal sediment bed. *Journal of Geophysical Research, 117*, F04015. doi: 10.1029/2012jf002490

Julien, P. Y., & Bounvilay, B. (2013). Velocity of rolling bed load particles. *Journal of Hydraulic Engineering, 139*(2), 177-186. doi: 10.1061/(asce)hy.1943-7900.0000657

Laganiere, R. (2011). *OpenCV 2 Computer vision application programming cookbook.* Birminghan, UK: Packt Publishing Ltd.

Lajeunesse, E., Malverti, L., & Charru, F. (2010). Bed load transport in turbulent flow at the grain scale: Experiments and modeling. *Journal of Geophysical Research, 115*, F04001. doi: 10.1029/2009jf001628

Le Roux, J. P. (2004). An integrated law of the wall for hydrodynamically transitional flow over plane beds. *Sedimentary Geology, 163*(3-4), 311-321. doi: 10.1016/j.sedgeo.2003.07.005

Lee, H. Y., & Hsu, I. S. (1994). Investigation of saltating particle motions. *Journal of Hydraulic Engineering, 120*(7), 831-845.

Meyer-Peter, E., & Muller, R. (1948). *Formulas for bed-load transport.* Paper presented at the Int. Assoc. Hydraul. Res., Stockhlom, Sweden.

Niño, Y., & García, M., H. (1994a). Gravel saltation 1. experiments. *Water Resources Research, 30*(6), 1907-1914.

Niño, Y., & García, M., H. (1994b). Gravel saltation 2. modeling. *Water Resources Research, 30*(6), 1915-1924.

Niño, Y., & García, M., H. (1998). Experiments on saltation of sand in water. *Journal of Hydraulic Engineering, 124*(10), 1014-1025.

Novak, P., & Nalluri, C. (1975). Sediment transport in smooth fixed-bed channels. *Journal of the Hydraulics Division, 101*(9), 1139-1154.

Papanicolaou, A. N., Diplas, P., Balakrishnan, M., & Dancey, C. (1999). Computer vision technique for tracking bed load movement. *Journal of Computing in Civil Engineering, 13*(2), 71-79. doi: 10.1061/(Asce)0887-3801(1999)13:2(71)

Papanicolaou, A. N., Knapp, D., & Strom, K. (2002, Jul 28 - Aug 1). *Bedload predictions by the using concept of particle velocity: applications.* Paper presented at the EWRI Int. conf. on Hydraulic Measurements and Experimental Methods, Estes Park, Colorado.

Parker, G. (2008). Transport of grvel and sediment mixtures. In M. Garcia (Ed.), *Sedimentation engineering: processes, measurements, modelling and partice* (pp. 165-251): ASCE.

Radice, A., Malavasi, S., & Ballio, F. (2006). Solid transport measurements through image processing. *Experiments in Fluids, 41*(5), 721-734. doi: 10.1007/s00348-006-0195-9

Ramesh, B., Kothyari, U. C., & Murugesan, K. (2011). Near-bed particle motion over transitionally-rough bed. *Journal of Hydraulic Research, 49*(6), 757-765. doi: 10.1080/00221686.2011.620369

Recking, A., Frey, P., Paquier, A., Belleudy, P., & Champagne, J. Y. (2008). Bed-load transport flume experiments on steep slopes. *Journal of Hydraulic Engineering, 134*(9), 1302-1310. doi: 10.1061/(asce)0733-9429(2008)134:9(1302)

Roseberry, J. C., Schmeeckle, M. W., & Furbish, D. J. (2012). A probabilistic description of the bed load sediment flux: 2. Particle activity and motions. *Journal of Geophysical Research-Earth Surface, 117*, F03032. doi: 10.1029/2012jf002353

Sekine, M., & Kikkawa, H. (1992). Mechnics of saltating grains. *Journal of Hydraulic Engineering, 118*(4), 536-558.

Tregnaghi, M., Bottacin-Busolin, A., Marion, A., & Tait, S. (2012a). Stochastic determination of entrainment risk in uniformly sized sediment beds at low transport stages: 1. Theory. *Journal of Geophysical Research-Earth Surface, 117*, F04004. doi: 10.1029/2011jf002134

Wu, F. C., & Yang, K. H. (2004). A stochastic partial transport model for mixed-size sediment: Application to assessment of fractional mobility. *Water Resources Research, 40*(4), W04501. doi: 10.1029/2003wr002256

Table 1 Characteristics of sediments used in experiments

Case	D_{50} (m)	Q (m^3s^{-1})	S	τ_* (Nm^{-2})	u_* (ms^{-1})	σ_g	Re_*	ρ_s (kgm^{-3})	H (m)
1	0.0015	0.00048 - 0.00164	0.0078 - 0.0227	0.069 - 0.113	0.045 - 0.057	1.225	90 - 144	2650	0.02 - 0.035
2	0.0024	0.00056 - 0.00172	0.0061 - 0.0236	0.037 - 0.093	0.038 - 0.060	1.296	108 - 138	2650	0.03- 0.037

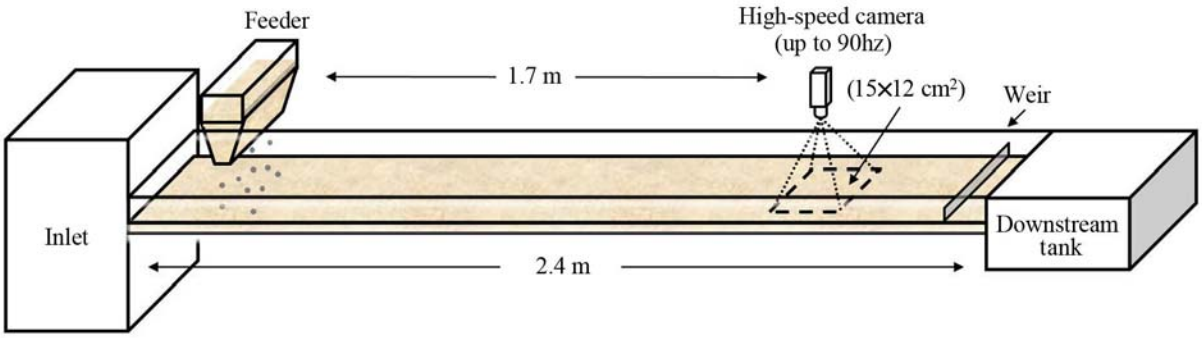

Fig. 1. Schematic of experimental setup

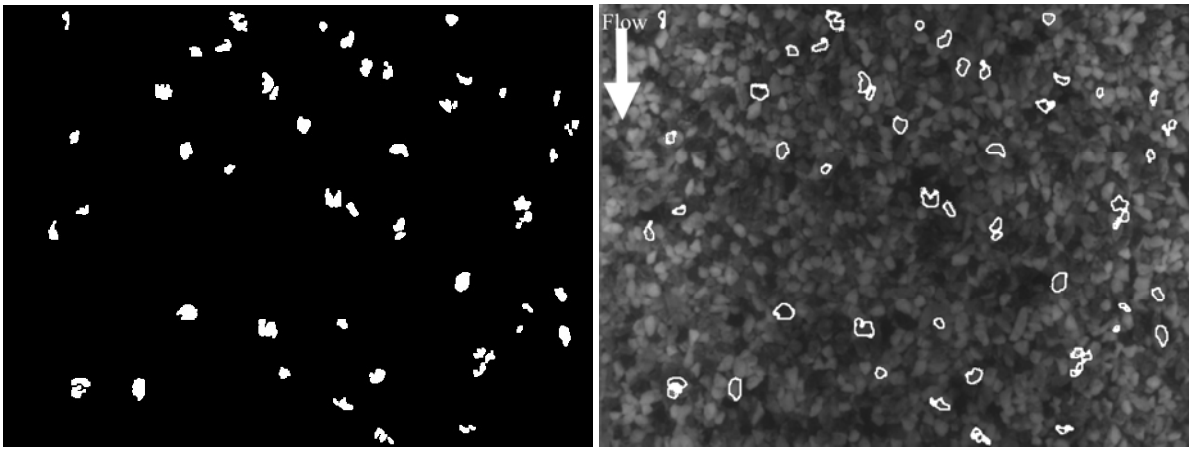

Fig. 2. Moving particle contour overlapped with origin image

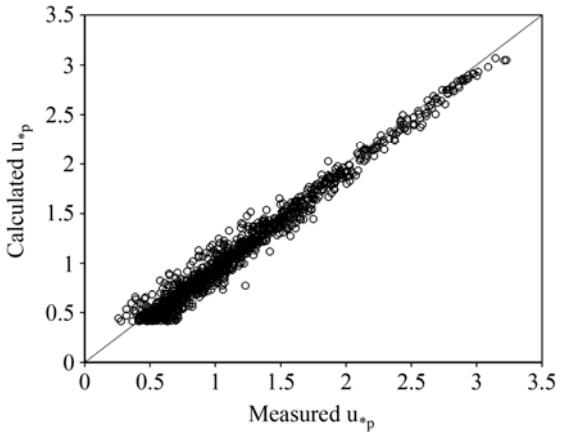

Fig. 3. Calculated dimensionless particle velocity verse the manually measure

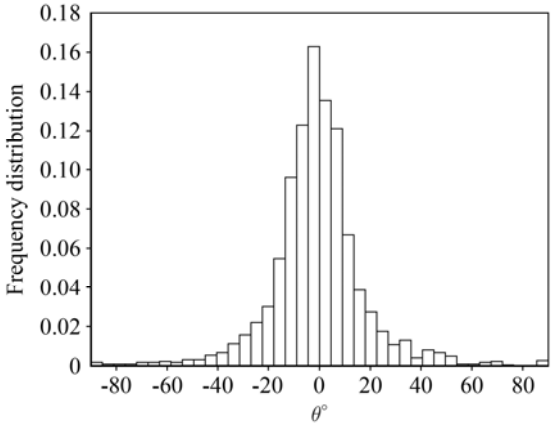

Fig. 4. Frequency distribution of orientation angles

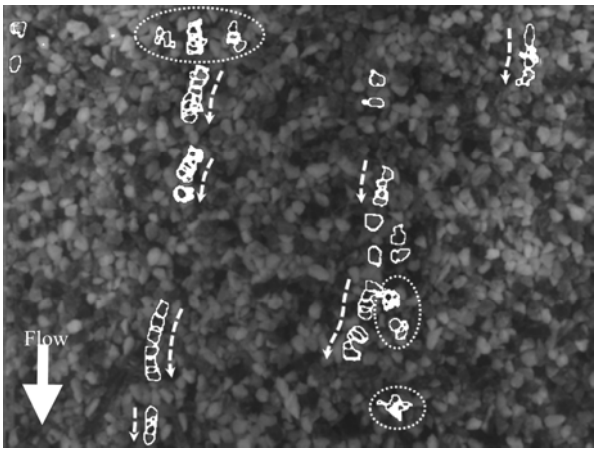

Fig. 5. Trajectories of moving particles for the particle size of 2.4mm (Case 2); the number of frame is 10 consecutive image. The arrow shows the trajectories of moving particles, and the circle area indicate shaking particles.

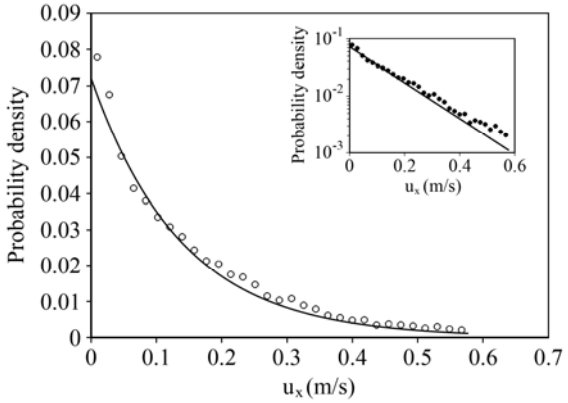

Fig. 6. Probability density function of streamwise particle velocity $u_x(m/s)$ with the particle size of 2.4 mm. Exponential PDF: circles are experiment data. Solid line represent Exponential distribution by equation (6)

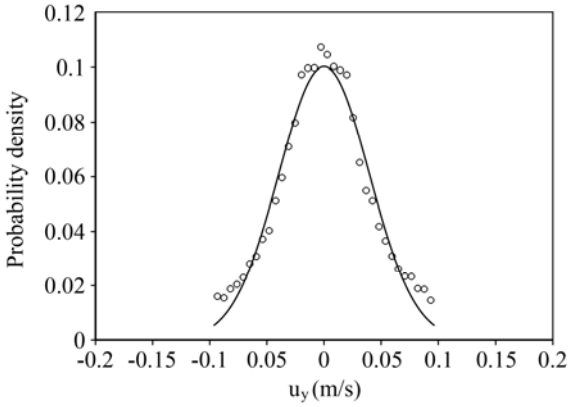

Fig. 7. Gaussian PDF of transverse particle velocity with the particle size of 2.4 mm. Circles are experiment data. Solid line represents Gaussian distribution by equation (7)

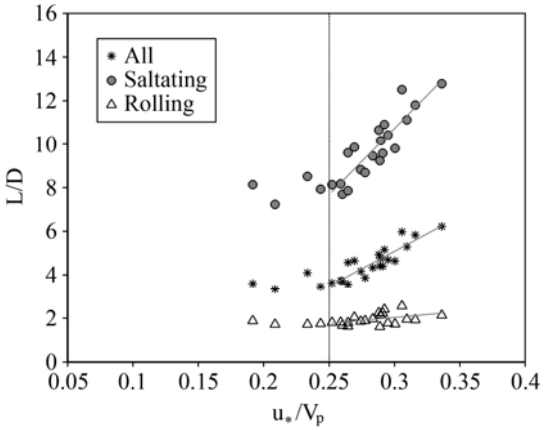

Fig. 8. Travel length of moving particle; all of moving particle, saltating and rolling

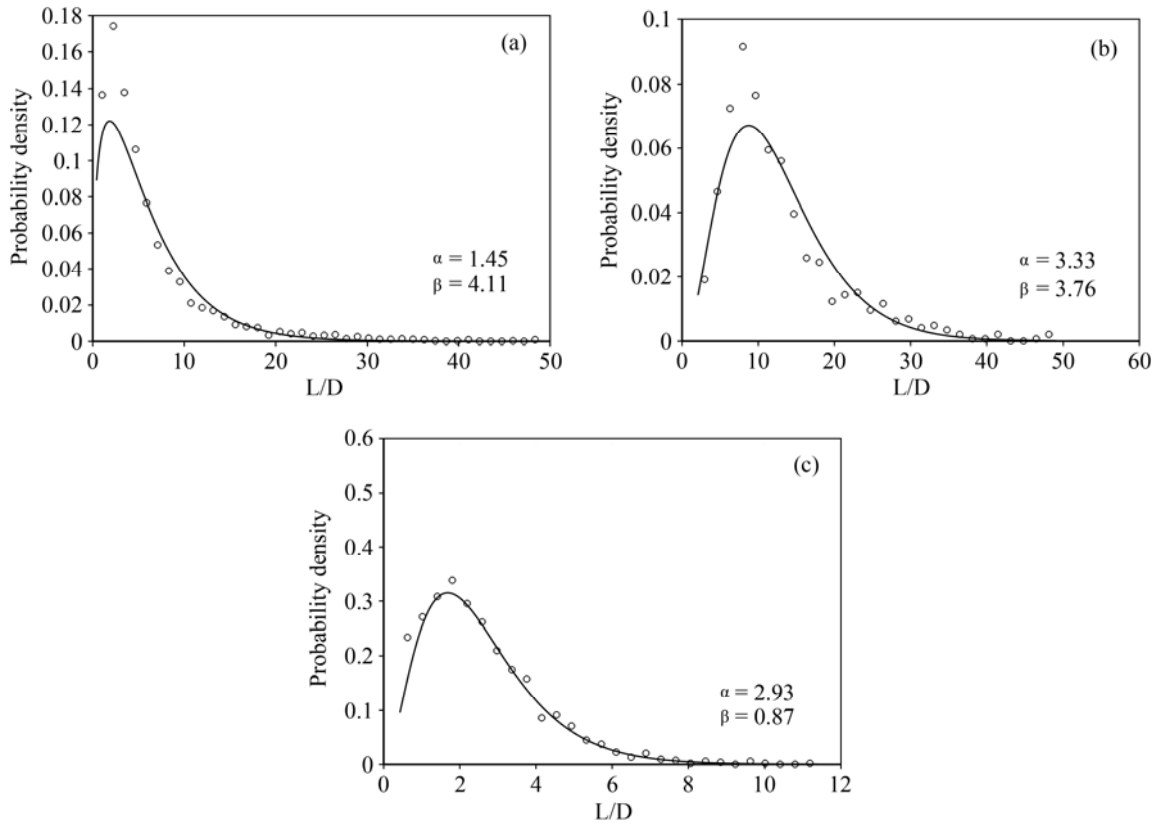

Fig. 9. Gamma PDF of the travel length: (a) all of moving particles (α=1.45, β=4.11 for 2.4mm), (b) saltating particles (shape and scale parameter for gamma PDF: α=3.33, β=3.76 for 2.4mm), (c) sliding/rolling particles (α=2.93, β=0.87 for 2.4mm)

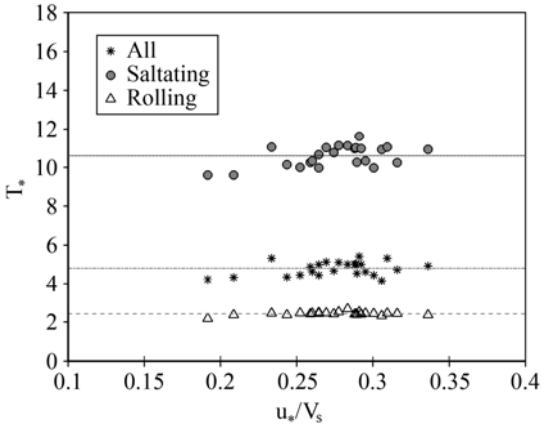

Fig. 10. Dimensionless travel time, each horizontal line represent liner fit of each data set

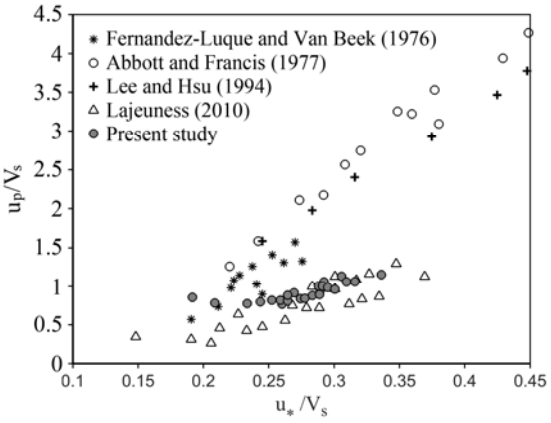

Fig. 11. Average particle velocity $\overline{u_p}/V_s$ versus u_*/V_s

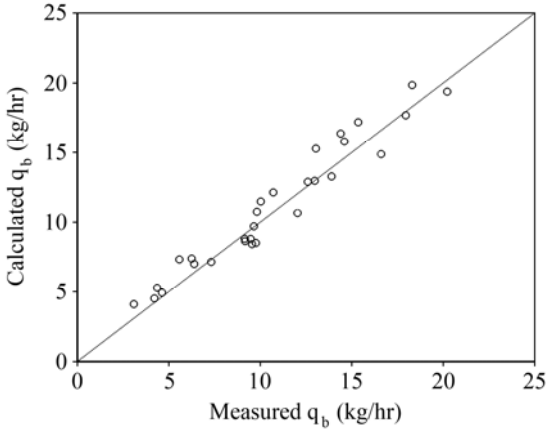

Fig. 12. Calculated sediment transport rate verse manually measured sediment transport rate

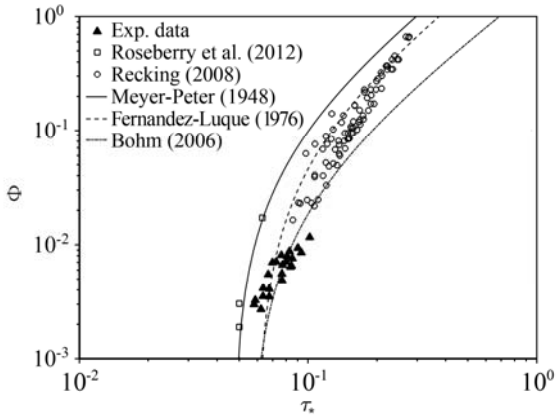

Fig. 13. Dimensionless transport rate versus Shields number; the experiment data by Recking (2008) and Rosebery et al. (2012), semi-empirical formulas (line) provided by Meyer-peter and Muller (1948), Fernandez-Luque and van Beek (1976) and Bohm (2006)

APPENDIX B - EXPERIMENTAL AND THEORETICAL STUDY OF BED LOAD PARTICLE VELOCITY

Jaeho Shim[1], Jennifer Duan[2]

Department of Civil Engineering and Engineering Mechanics, University of Arizona, Tucson, AZ 85721, USA

Abstract

This paper reported an experimental study of sediment particle velocity in the Hydraulic Engineering Laboratory at the University of Arizona. The experiments were performed in a rectangular channel filled with a layer of coarse sand or gravel. The instantaneous particle velocity was measured by using the images captured with a commercial camera. An innovative image processing technique was developed for tracking individual particle motion, which leads to the determination of instantaneous particle velocity vector. Both the mean particle velocity and the distribution of particle velocities were analyzed. It was found that the instantaneous bed shear stress dominate the particle velocity as well as the probability density function of its distribution. This observation is consistent with the theoretically derived equations for particle velocity and its distribution. Furthermore, the Kolmogorov-Smirnov test confirmed the agreement between the distribution of experimental data and that obtained from the theoretical analysis.

Keywords: Shear stress intensity, Particle velocity, Stochastic model, Probability distribution

1. Introduction

Bed load transport rate is the amount of bed load particles transported along with flow on the bed surface. It can be quantitatively measured as the volume or the mass of bed load particles passing through a unit width of a cross section within a time period. Theoretically, to determine bed load transport rate, one needs to measure the velocity of each bed load particle. Due to irregular shapes, non-uniform sizes, and the randomness of particle motion, each particle has a distinct

velocity at a given time and space. Besides, it's well know the thickness of bed load layer is more than one particle diameter, which means some moving particles are visible on bed surface, and some are hidden underneath. Furthermore, the mode of bed load particle motion can be rolling, sliding, and saltation, which makes the measurements of particle velocity even more challenging. Up to now, no method is capable of measuring the velocity of each bed load particle. To calculate bed load transport rate, researchers often use the average velocity of all the moving particles, and assume that this average velocity is only dependent on particle size and flow properties. Its shape, irregularity, orientation to flow on bed surface, and buried depth were assumed not to affect the average particle velocity. Therefore, in earlier dates, researchers [1-9] measured the velocity of an individual particle by tracking its trajectory either on fixed or mobile bed, and this velocity was assumed as the approximation of the average particle velocity. Because the saltation motion has a relatively large step length, particle trajectories are easier to be identified in the images, researchers often derived the mean properties of saltation motion. For example, Fernandez Luque and Van Beek [5] measured mean number of moving particle per unit and the average length of individual particle step on mobile bed using 16 frame rates camera. Abbott and Francis [6] used a high speed camera to capture the images of single particle motion over a fixed bed surface. Not only the average particle velocity but also the average saltation length and height were obtained by averaging over the selected particles. Bridge and Dominic [1] obtained the velocity of a single saltation particle using its trajectory, and also derived an equation for calculating the average particle velocity on a fixed rough bed. Van Rijn [8] found the majority of bed load particles were transporting as saltation motion, and then derived a single-step saltation particle model for bed load transport at low Reynolds number.

Wiberg and Smith [9] studied the mechanism of saltation particle processes, and proposed a numerical model for the motion of a single saltation particle using the impacting and rebounding physical mechanism. Sekine and Kikkawa [2] found a single saltation particle velocity is a function of friction velocity and sediment fall velocity. Lee and Hsu [3] analyzed the continuous images of saltation for their trajectories and velocities, and developed a mathematical model to simulate motion of a single saltation particle. Niño and García [4] and Niño and García [7] used high speed camera to captured the number of saltating particles moving, also applied a mathematical model to study the average saltation velocity and bed load transport rate. Using previous researches data, some regression analyses for motion of bed load particles have been done by Cheng and Emadzadeh [10], and Julien and Bounvilay [11].

Despite many benchmark studies using a single particle [1-3, 5, 6, 12], one major concern is that neither an individual particle nor a group of manually selected particles can sufficiently represent the mean properties of all the moving particles on the mobile bed surface. It's obvious that the statistical properties of particle velocity can only be obtained from the measurements of all the moving particles. The high-speed camera can capture consecutive images of all the moving particles, and the moving distance between two consecutive images can be extracted [13-15]. Lajeunesse [13] and Houssais and Lajeunesse [14] used Particle Tracking Velocimetry (PTV) to investigate the average velocity, density, and transport rate of moving particles. However, the camera based approaches can only measure the velocities of particles on bed surface, and particles hidden under the topmost layer were not captured. Comparing to previous methods in which a single or a few particles were measured on a fixed bed, it's a better representation of all the moving particles. To simply the analysis, researches often account for a

number of selected particles instead of all the moving particles in an image when calculating the average particle velocity. This treatment was adopted because it's difficult to identify and track each individual particle when processing thousands of images either manually or by commercial software (e.g., ImageJ). Consequently, researchers[16-20] used selected particles from these images to study the properties of bed load particle motion. Furbish [16] applied an imaging technology (ImageJ) to measure bed-load particle transport, and derived a probabilistic formulation for particle velocity in turbulent flow. Tregnaghi [17] noted that the fluctuation of fluid force, grain resistance, and geometrical configuration of the mobile bed surface are the key factors for determining particle velocity. Valyrakis [18] showed that fluctuation of turbulence influences the characteristics of saltation and life and drag forces acting on the particles fluctuate with respect to time. Armanini [19] presented a theoretical approach to evaluate sediment transport rate using the averaged particle velocity and a probability density function for the particle travel length. Ancey and Heyman [20] also observed the randomness of moving particles in their experiment and applied a stochastic model describing particle motion using the frame work of birth-death Markov processes. Cheng and Emadzadeh [10] summarized 14 formulas for calculating bed load particle velocity. Because of different datasets used for deriving these formulas, there is no consensus on the average bed load particle velocity, as well as the probability density function (PDF) function for its distribution.

This study aims to use the instantaneous velocities of all the moving particles to obtain the average and statistical properties of bed load particle velocity using a newly developed video image based Particle Tracking technique (VIPT). This technique is capable of capturing a number of continuous moving particles simultaneously, and automatically calculating particle

geometric properties and particle velocities [21, 22]. This present study extends the previous preliminary research of Shim and Duan [23], and derived analytical formulas for mean particle velocity and its density distribution function by treating bed-shear stress as a stochastic variable. Laboratory experiments were conducted to verify the theoretically derived equations, and the captured images were processed using the VIPT software [24].

2. Theoretical Development

2.1 Mechanics of particle motion

For a single particle residing on bed surface, the external forces exerted on its body are the drag and friction forces in the horizontal plane, and the lift and gravity forces in the vertical direction. Fig. 1 is the free body diagram for a moving bed load particle. The drag force is the fluid induced bed shear stress in the direction of particle transport. Bed load particles move mostly in contact with the bed surface, but may experience brief periods in the fluid. The friction force is the total resistance force on individual particle consisting of the skin resistance, form resistance due to pressure differences on the particle surface, and extra force from inter granular collisions or particle striking on bed surface. In the vertical direction, the lift force is important to keep the bed load particle stay in the flow while being transported, and it's approximately equal to the buoyancy force [5]. As a bed load particle completes a motion, it strikes bed surface and lose about 85% of the streamwise particle velocity. Therefore, the averaged bed load particle velocity accounting for the reduction of particle momentum at the end of each motion is smaller than the average particle velocity while suspended in the fluid. In this study, we captured the images of all the moving particles on bed surface including those in suspension, striking on bed surface,

and just being entrained from bed surface. The average particle velocity obtained from two consecutive images is the average of all the moving particles on the horizontal plane. At any moment, in the streamwise direction, the total external forces on an individual sediment particle are equal to the product of its mass and acceleration based on the Newton's law, which is written as:

$$F = ma = F_d - F_f \tag{1}$$

where F is the sum of the drag and friction forces, m is the mass of uniform sized particle , a is acceleration, and F_d and F_f are the instantaneous drag and friction forces, respectively. The instantaneous drag force on each particle is the same bed shear stress (τ), which can be calculated by the velocity distribution in the vertical direction. The instantaneous friction force on each particle is dependent on the stage of particle motion in rolling, sliding, or saltation. For example, if the saltation particle is striking the bed surface, the friction force can be simplified as the reduction of momentum per unit time over one step length of a particle motion. This is analogous to the calculation of turbulent shear stress reduction due to particle motion in Fernandez Luque and Van Beek [5]. However, if the particle is sliding on bed surface, the friction force relates to bed surface roughness and the weight of particle. There is not a single mathematic function that can be used to calculate the instantaneous friction force on a particle. Therefore, this friction force was assumed to be proportional to the reduction of momentum over one particle motion. This assumption will over-estimate the friction force, so that a coefficient, $\theta < 1$, was multiplied to the reduction of momentum. The friction force is calculated as:

$$F_f = \frac{\theta \Delta M_s}{\Delta t_s} = \frac{\theta(\rho_s + C_M \rho_f)\Delta u_p c_1 D_s^3}{\lambda_s / \overline{u}_b} \tag{2}$$

where ΔM_s is the reduction of momentum in one step length, ρ_s and ρ_f are the densities of sediment and flow, respectively, $C_M \rho_f c_1 D_s^3$ is the added mass due to flow around particles, C_M = 0.5 for the spherical particles, c_1 is the coefficient for approximating the volume of a sediment particle, Δu_p is the reduction of particle velocity in the streamwise direction in one motion, Δt_s is the duration of a step, λ_s is the distance traveled in a step, and $\overline{u}_b$ is the averaged particle velocity over one step length. The velocity reduction of sediment particles in the streamwise direction Δu_p is assumed to be a fraction of instantaneous particle velocity, u_p, on the bed surface, similar to that in [5].

$$\Delta u_p = \alpha u_p \tag{3}$$

The step length of one particle motion, λ_s, is proportional to particle diameter, D_s,and defined as

$$\lambda_s = D_s \lambda_{s*} \tag{4}$$

where D_s is the size of sediment particle, and λ_{s*} is the ratio between the step length and particle size, named the dimensionless step length. Substituting Eqs. (3) and (4) into Eq. (2), the friction force becomes

$$F_f = \frac{\alpha \theta c_1 (\rho_s + C_M \rho_f)\Delta u_p D_s^3}{D_s \lambda_s / \overline{u}_b} \tag{5}$$

Substituting the drag force, $F_d = \tau A$, and the friction force in Eq. (5) into Eq. (1), it follows

$$\frac{du_p}{dt} = \frac{\tau A}{m} - \frac{\alpha\theta\bar{u}_b}{D_s\lambda_{s*}}u_p \tag{6}$$

where A is the particle surface area projected to the horizontal plane. In Eq. (6), the average particle velocity over a step length was taken as a fraction of instantaneous particle velocity, $\bar{u}_b = \beta u_p$. Therefore, Eq. (6) can be simplified as

$$\frac{du_p}{dt} = \frac{\tau A}{m} - \frac{\alpha\beta\theta c_1}{D_s\lambda_{s*}}u_p^2 \tag{7}$$

Eq. (7) is a non-linear ordinary differential equation. The surface area for a particle is approximated as $A = c_2 D_s^2$ in which c_2 is an coefficient. The particle mass including the added mass by fluid can be written as $m = c_1(\rho_s + C_M\rho_f)D_s^3$. Using the initial condition at t=0, u_p=0, the solution for the particle velocity is:

$$u_p = \sqrt{\frac{k_1}{k_2}}\left(\frac{1 - \frac{1}{e^{2\sqrt{k_1 k_2}t}}}{1 + \frac{1}{e^{2\sqrt{k_1 k_2}t}}}\right) \tag{8}$$

where

$$k_1 = \frac{\tau A}{m} = \frac{c_2\tau}{c_1(\rho_s + C_M\rho_f)D_s} \qquad \text{and} \qquad k_2 = \frac{\alpha\beta\theta c_1}{D_s\lambda_s} \tag{9}$$

At $t = \infty$, the equilibrium state of bed load transport is reached, and Eq. (8) yields the solution of particle velocity at the equilibrium transport:

$$u_p = \sqrt{\frac{k_1}{k_2}} = \sqrt{\frac{\lambda_{s*}}{\eta(\rho_s + C_M \rho_f)}\tau} \quad \text{in which } \eta = \frac{\alpha\beta\theta c_1^2}{c_2} \tag{10}$$

The coefficient, η, in Eq. (10) is a composite factor accounting for the particle shape factor, the momentum change, and particle averaged velocity over a step length. From Eq. (10) , the ultimate particle velocity at the equilibrium transport state is determined by bed shear stress, dimensionless step length, and particle size. Bed shear stress is a random variable depending on near bed turbulence, and the dimensionless step length is also a random variable depending on the mode of particle motion (e.g., sliding, rolling, saltation). Because of this, the particle velocity at the equilibrium transport is a random variable depending the randomness of particle motion mode and near bed turbulence. At an instant, bed shear stress is the same on all the moving particles, but particle velocity varies spatially due to its size, position, shape, angularity, and others. The average velocity of all the moving particles at one instant is called the spatial average particle velocity. At the equilibrium transport, it is the average of Eq. (10), in which the shear stress only varies with time but not space:

$$\overline{u}_p = \sqrt{\frac{\lambda_{s*}}{\eta\left(\rho_s + C_M \rho_f\right)}\tau} \tag{11}$$

Eq. (11) shows the spatial average particle velocity at the equilibrium transport state is a function of dimensionless spatial step length and the instantaneous bed shear stress. Many studies [1, 3, 5-7, 25, 26] have measured the particle saltation length of an individual particle on a fixed bed, and a few on mobile bed. A few recent experiments measured the average particle saltation length on mobile bed [13, 14, 27]. The step length for saltation particle is much larger than that of sliding and rolling ones. Shim and Duan [28] found the saltation length ranges from 6 to 14

particle diameters, while rolling and sliding length is 2-8 particle diameters. Other studies found the saltation length can be 100 particle diameter [29]. At low shear stress, bed load particles are sliding or rolling on bed surface, while at high shear stress, more particles are in saltation motion. Therefore, the dimensionless average step length (λ_{s*}) is a function of dimensionless mean shear stress, τ_* / τ_{*c}. If the average bed shear stress is high on a particle, the particle will transport a longer step, vice versa. Among the experimental data, [5] and [12] are the only ones performed on the mobile bed. In both experiments, selected particles were used to find the average saltation length and particle velocity at a given flow condition. There are two sets of experiments that measured the step lengths of rolling and sliding particles on a fixed bed. Therefore, we selected all the measured data, and the correlation $\overline{\lambda}_{s*}$ vs τ_*/τ_{*c}, was shown in Fig. 2, a linear relationship was obtained as

$$\overline{\lambda}_{s*} = a(\tau_*/\tau_{*c}) + b \tag{12}$$

where $a = 3.1$ and $b = 0.45$. We must bear in mind that these two coefficients are based on the experimental data of selected saltation particles on either fixed or mobile bed, which are not an accurate representation of all the moving particles. Therefore, the coefficients in Eq. (12) remain as unknowns for all the moving particles. Then, substituting Eq. (12) into Eq. (10), the spatial average particle velocity at the equilibrium transport is expressed as the dimensionless shear stress.

$$\overline{u_p} = \sqrt{\frac{(SG-1)gD_s}{(SG+C_M)}(\omega_1 \frac{\tau_*}{\tau_{*c}} + \omega_2)\tau_*} \tag{13}$$

where $SG = \rho_s / \rho$, is specific gravity. The coefficients, $\omega_1 = \frac{a}{\eta}, \omega_2 = \frac{b}{\eta}$,, +will be determined by curve fitting the experimental data from this study and prior experiments. Equation (13) shows the spatial average particle velocity at the equilibrium transport is a function of instantaneous bed shear stress. The time average of $\overline{u}_p$,denoted by $\overline{\overline{u}}_p$, is only dependent on the time average of bed shear stress, symbolized as $\overline{\tau}_*$:

$$\overline{\overline{u}}_p = \sqrt{\frac{(SG-1)gD_s}{SG+C_M}\left(\omega_1 \frac{\overline{\tau}_*}{\tau_{*c}} + \omega_2\right)\overline{\tau}_*} \tag{14}$$

Eq. (14) is the equation for spatial and temporal averaged particle velocity at the equilibrium transport. For a given shear stress, this average particle velocity is a function of mean shear stress and particle size.

2.2 Distribution Function of Particle Velocity

At the equilibrium transport state, the spatial average particle velocity is only dependent on instantaneous bed shear stress and particle size. Studies have shown that the dynamics of individual bed load sediment particle is driven by the near-bed turbulence burst, especially sweep and ejection events [24, 30]. Consequently, the bed shear stress varies instantaneously with time. At one instant, bed shear stress is the same on all the moving particles regardless of particle locations, orientation, and sizes. The averaged particle velocity at this instant, named, spatially averaged particle velocity, is only depend on the instantaneous shear stress. Therefore, the spatial averaged particle velocity is believed to be dependent on the instantaneous bed shear

stress [31, 32]. The PDF of the instantaneous shear stress on the bed surface was found to satisfy a standard log-normal distribution [31, 33] as:

$$f(\tau)=\frac{1}{\sqrt{2\pi}\sigma_{\ln\tau}\tau}\exp\left[\frac{-\left(\ln\tau-E_{\ln\tau}\right)^2}{2\sigma_{\ln\tau}^2}\right] \qquad \tau\geq 0 \tag{15}$$

where $E_{\ln\tau}$ and $\sigma_{\ln\tau}$ denote the mean and standard deviation of the random variable $\ln\tau$. The mathematical mean and standard deviation of τ are written as [34];

$$E_\tau=e^{E_{\ln\tau}+\left(\sigma_{\ln\tau}^2/2\right)} \quad \text{and} \quad \sigma_\tau=E_\tau\sqrt{e^{\sigma_{\ln\tau}^2}-1} \tag{16}$$

The relation between the mathematical mean and standard deviation of τ and $\ln\tau$ can be written as follows [33];

$$E_{\ln\tau}=\ln\frac{E_\tau}{\sqrt{1+I_\tau^2}} \quad \text{and} \quad \sigma_{\ln\tau}=\sqrt{\ln(1+I_\tau^2)} \tag{17}$$

where $I_\tau=\sigma_\tau/E_\tau$ denotes the relative intensity of bed-shear stress. Therefore, from Eq. (17) and Eq. (2), the PDF of bed-shear stress is only a function of the relative intensity of bed shear stress, which is denoted by I_τ. The mathematical expression of the bed shear stress distribution is shown below

$$f(\tau)=\frac{1}{\sqrt{2\pi\ln(1+I_\tau^2)}\tau}\exp\left[\frac{-\left(\ln\tau\sqrt{1+I_\tau^2}/E_\tau\right)^2}{2\ln(1+I_\tau^2)}\right] \tag{18}$$

Cheng and Law [33] analyzed experimental data published in [35], [36], [37], [38] and studied the relation between Reynolds number and bed-shear stress intensity. From the experimental data, an empirical relation can be formed as Cheng and Law [33]:

$$I_\tau = \alpha_\tau (\mathrm{Re})^{\beta_\tau} \tag{19}$$

where $\mathrm{Re} = VR/\nu$ is flow Reynolds number calculated by the average flow velocity (V), hydraulic radius (R) , and kinematic viscosity (ν). Fitting the data using the least square method yields $\alpha_\tau = 150$ and $\beta_\tau = -0.671$, respectively, for the relative intensity of bed shear stress, $0.25 < I_\tau < 1.2$. The results of Cheng and Law [33] and Cheng [31] showed that the value of I_τ increases as Reynolds number is reduced, however there are no measurements for Re>12,000. Duan and Barkdoll [34] assumed that I_τ continues to decrease as Reynolds number increases, so that Eq. (18) is valid for Re > 12,000.

Since the probability distribution of bed shear stress satisfies the log-normal distribution [23], the spatial averaged particle velocity at the equilibrium transport should also satisfy the long-normal distribution. The PDF of particle velocity can be obtained using Eq. (13) by treating the bed shear stress as a random variable of the log-normal distribution (Eq. 18). In the following section the theoretically derived equation, Eq. (14) for the spatial and temporal average particle velocity and the PDF of spatially averaged particle velocity (Eq. 13), will be verified later in this paper by data from several experiments.

3. Laboratory Experiment

3.1 Experiment setup

The experiments for this study were performed in a 0.15 m wide and 2.4 m long rectangular recirculating titling flume filled with approximately 3 cm of sediment on the bed as shown in Fig.3. The flow was delivered by a pump from a tank, and controlled by a valve on the pipe.

Water enters the flume into a tank at the front of a flume, and metal sheet was placed at the inlet to stabilize flow. In this study, weir was used for regulating the flowrate before the experiment. A rating curve between flow discharge and flow depth upstream of the weir was pre-determined. The measured flow depth upstream of the weir was used to determine flow discharge in the flume. Flow discharge was remained as a constant in each experiment. Water exited the flume into the tank, and then was pumped back into the flume. After determined discharge, weir was removed and flow depth was regulated by a tailgate installed at the end of the flume. When flow depths measured at the front, center, and end of the flume are within 0.5 mm difference, flow is considered as steady uniform. Then, camera was activated to take a series of consecutive images.

The measurement section is located 1.7 m from the inlet on the centerline of the flume. A Sony commercial camera, Model XCD-V60, was installed above the measurement area, which is capable of taking images at a resolution of 640×480 pixels with a rate up to 90 fps. To remove the distortion by light reflection, a plastic plate was floating freely on the water surface. Figure 3 also shows the location of the test section and the camera. In each run, over 1,300 consecutive images were taken at 90 fps in about 16 seconds. Because of the limitation of the camera focus lens, the camera captured an image of 200 mm × 150 mm rectangle viewing window. During the experiment, sediment was fed into the flume externally at the entrance to ensure steady uniform flow conditions. The feeding rate is approximately the transport rate measured at the end of the flume. This was achieved by feeding at the entrance with all the sediment collected at the flume end. Two uniformly sized sediments with sizes: d_{50} : 1.5mm and 2.4 mm, and a density of ρ_s = 2,650 kg/m^3, were used. A total of 23 runs were performed in this study.

Since flow is steady and uniform, the streamwise bed shear stress is approximated by

$$\tau = \rho g R S \tag{20}$$

where ρ is water density. The energy slope (S) is approximated by the bed surface slope measured by an inclinometer with an accuracy of 0.1°. Flow depth is measured by a fine scaled ruler (1.0 mm) glued on the flume side. The shear stress, τ_*, and the shear velocity are calculated by

$$\tau_* = \frac{\tau}{g(\rho_s - \rho)D_s} \tag{21}$$

$$u_* = \sqrt{\frac{\tau}{\rho}} = \sqrt{gRS} \tag{22}$$

where, u_* is friction velocity. The critical shear stress is calculated as $\tau_c = \tau_{*c}(\gamma_s - \gamma)D_s$, in which $(\gamma_s - \gamma)$ is the submerged specific weight of sediment. The critical shear stress for sand-gravel sized sediment is obtained using the Shield's diagram. A constant value of critical shear stress $\tau_{*c} = 0.031$ for Re_* ranging from 70 to 150 is used in this study [39]. Details were summarized in Table 1.

3.2 Image processing

A particle tracking algorithm was developed to track particles' trajectory Shim and Duan [22] using the motion detection algorithm in OpenCV Library (http://code.opencv.org). At first, the captured digital picture images were converted to binary images for processing. Secondly, each moving particle was identified and isolated by a motion detecting algorithm based on image

subtraction. It was performed by background subtraction between consecutive images to detect any moving particles in the frame. Thirdly, each image was processed by using morphological erosion and dilation transformations. This erosion and dilation process allows all the identified moving particles to have a distinct particle shape. After this process, a binary image of a moving particle was obtained, and then the x- and y- coordinates of each particle were calculated as well.

Several criteria were applied to track a particles' trajectory. The first criterion is to use the particle size, which was compared with the original one in the searching area, through its particle size ratio. Another criterion is the color information within each particle. Using the origin image overlapped with the outline of moving particles, the histogram of color within each outline of moving particle was extracted. The third criterion is to measure the minimal distance between the moving particles. These distinctive parameters of particles were used together to track the particle in the consecutive images. The best match is considered to be the location of the tracking particle. This image processing technique is capable of accurately detecting all the moving particles so that their instantaneous velocities can be calculated by comparing two consecutive images. These measurements were the database for calculating the statistical properties.

4. Verification of Theoretical Equations

4.1 Particle velocity

The averaged particle velocity was calculated by Eq. (14), and non-dimensionlized using Eq. (23). A similar method was used in Sekine and Kikkawa [2].

$$\overline{\overline{u_{*p}}} = \frac{\overline{\overline{u_p}}}{\sqrt{(SG-1)gD_s}} \tag{23}$$

Then, the dimensionless spatial and temporal averaged particle velocity can be obtained by substituting Eq. (14) into Eq. (23) as:

$$\overline{\overline{u}}_{*p} = \sqrt{\frac{1}{SG + C_M}\left(\omega_1 \frac{\overline{\tau}_*}{\tau_{*c}} + \omega_2\right)\overline{\tau}_*} \tag{24}$$

Using the experimental data from this study to fit Eq. (24), the best curve fit is shown in Fig. 4, in which the dimensionless shear stress $\tau_{*c} = 0.031, \omega_1 = 26.3, \omega_2 = 34.6$. The correlation coefficient for the fitted polynomial function is 0.8761. Eq. (24) is the dimensionless particle velocity at a given bed shear stress and particle size. The dimensionless critical shear stress can be obtained by using the Shield diagram. The coefficients are obtained from the experimental data in this study. The applicability of this equation and the comparison with other equations are detailed in the discussion session.

4.2 Two sample Kolmogorov-Smirnov test

The two sample Kolmogorov-Smirnov (K-S) test was adopted to examine the agreement between the distribution of experimental data and that obtained from the theoretical equation (Eq. 13) by treating the bed shear stress as a random variable. The K-S test reports the maximum difference between two cumulative distribution functions, symbolized by $D_{m,n}$ [40, 41].

$$D_{m,n} = \max\left|F_m(x) - G_n(x)\right| \tag{25}$$

where $F_m(x)$, denotes the observed cumulative distribution function (CDF) with a sample size, m, and $G_n(x)$ is the calculated cumulative distribution function with a sample size, n. In the K-S test, the null hypothesis (H_0) assumes that both the samples come from a population with the

same distribution. If the value ($D_{m,n}$) is greater than the critical value ($D_{m,n,\alpha}$) at a significance level (α), the K-S test rejects the null hypothesis, which concludes that the calculated distribution does not properly fit the observed data. The critical value is determined by the selected significance level (α) and the sample size [42]. If the sample size *m* and *n* are sufficiently large, α =0.05 (5% significance level) is commonly used, and the corresponding critical value is $D_{m,n,0.05} = 1.36\sqrt{(m+n)/mn}$.

For all the experimental runs, the measured cumulative distribution of u_p from each run was compared with the one calculated using Eq. (15) by treating the bed shear stress as a random variable. The maximum difference between the calculated and measured values ($D_{m,n}$) were obtained. For example, Fig. 5 shows the K-S test results for Run #2. $D_{m,n} = 0.0752$. At the 5% significance level, $D_{m,n} < D_{m,n,0.05}$=0.1026, therefore the null hypothesis was accepted, and the measured particle velocity distribution from Run #2 satisfies the distribution using Eq. (13). The results of the K-S test for all the runs are summarized in Table 2. The values of $D_{m,n}$ from all the runs are smaller than the critical values ($D_{m,n,\alpha}$). These results indicate that the hypothesis is true for all the runs, which confirms that the particle velocity distribution satisfies the lognormal distribution. However, previous studies [13, 27] have advocated that particle velocity matches well with the exponential distribution. In the next section, it is explained that the exponential distribution is only valid at low Reynolds number when turbulence intensity is high.

4.3 Variation of particle velocity distribution with turbulence intensity

In Eq. (17), the distribution function of bed shear stress is a function of turbulence intensity. The

Reynolds numbers for 23 experimental runs range from 4,800 to 18,000, and the relative intensities (I_τ) are between 0.21 and 0.51 as shown in Table 1. In Fig. 6, the calculated PDFs of particle velocity (solid lines) for four experimental runs with various turbulence intensities (0.24 ~ 0.51) were compared with the measurements (bars). When the turbulence intensity is small, the distribution is log-normal. As the turbulence intensity increases, the PDFs became spiked and closer to the exponential distribution.

This is consistent with the observations in Lajeunesse [13] and Roseberry [27], who found the exponential-like (e.g. gamma distribution) PDF for streamwise particle velocity. The experimental runs in Lajeunesse [13] have relatively low Reynolds numbers (Re < 6000), and Roseberry [27] used very fine sand (0.5 mm). Reynolds numbers for the experiments in this study range from 4,800 to 18,000, and the median sediment sizes are coarser, 1.5mm and 2.4 mm, respectively.

Fig. 7 shows the changes of log-normal distribution function with the relative intensity of bed shear stress. At low Reynolds number, the I_τ value is large, and the log-normal and exponential distributions are nearly the same. This is perhaps the reason that other studies found the distribution function matched the exponential distribution. As Reynold number increases, turbulence becomes more dominant and the I_τ value reduces. As this occurs, the distribution deviates from the exponential distribution, but remains consistent with a log-normal distribution. The log-normal distribution matched the measured data much better than the exponential distribution, especially at high Reynolds number. Therefore, this study suggests the log-normal instead of the exponential distribution as the PDF of particle velocity. At present, our

experimental data are only limited to particle transport at low shear stress, we expect that this method will be applicable to flows with high sediment transport rate by using cameras with a sampling frequency of 500-1000 Hz.

5. Conclusion

This paper reported an experimental and theoretical study of the average bed load particle velocity and its distribution. A theoretical equation was derived for calculating the particle velocity and distribution at the equilibrium transport state. It was found the mean particle velocity is a function of average bed shear stress, and the instantaneous velocity of a bed load particle is dependent on the instantaneous bed-shear stress. The PDFs of particle velocity and bed shear stress both vary with the turbulence intensity. To verify this, a series of laboratory experiments were performed, and particle velocity was measured using a new image-processing technique. The two sample Kolmogorov-Smirnov (K-S) test was conducted to examine the agreement between the cumulative distributions of experimental data and distributions obtained from the theoretical model. Results showed that the newly derived theoretical equation accurately predicted the average particle velocity. The PDF of particle velocity is a log-normal function at high Reynolds number, while it is close to an exponential distribution at low Reynolds number.

Acknowledgements

This research is supported by the United States National Science Foundation Award CMMI 1434923.

Nomenclature

A	particle surface area
a	acceleration
$D_{m,n}$	maximum difference between two cumulative distribution
$D_{m,n,\alpha}$	critical value at a significance level (α)
D_s	particle size
E_τ, $E_{\ln\tau}$	mean of the random variable τ and $\ln\tau$
F	sum of the drag and friction forces
F_d, F_f	drag and friction force
$F_m(x)$	observed CDF with a sample size *m*
$G_n(x)$	calculated CDF with a sample size *n*
H_0	null hypothesis
I_τ	relative intensity of bed shear stress
m	mass of particle
R	hydraulic radius
Re	Reynolds number
S	bed surface slope
SG	specific gravity
u_b	average particle velocity over one trajectory
u_p	instantaneous particle velocity

V	flow velocity
γ, γ_s	specific weight of water and sediment
ΔM_s	reduction of momentum in one saltation length
Δt_s	duration of a saltation step
Δu_p	loss of streamwise particle velocity
λ_s	step length of saltation
λ_{s*}	dimensionless saltation length
ν	kinematic viscosity
ρ, ρ_s	density of water and sediment
$\sigma_{\ln\tau}$	standard deviation of the random variable $\ln\tau$
σ_τ	standard deviation of the random variable τ
τ	bed shear stress
τ_c	critical shear stress
τ_*	dimensionless shear stress
τ_{*c}	dimensionless critical shear stress
$\forall_p$	particle volume

References

[1] Bridge JS, Dominic DF. Bed load grain velocities and sediment transport rates. Water Resour Res. 20 (1984) 476-90, http://dx.doi.org/10.1029/Wr020i004p00476.

[2] Sekine M, Kikkawa H. Mechnics of saltating grains. J Hydraul Eng. 118 (1992) 536-58.

[3] Lee HY, Hsu IS. Investigation of saltating particle motions. J Hydraul Eng. 120 (1994) 831-45.

[4] Niño Y, García M, H. Gravel saltation 2. modeling. Water Resour Res. 30 (1994b) 1915-24.

[5] Fernandez Luque R, Van Beek R. Erosion and transport of bed-load sediment. J Hydraul Res. 14 (1976) 127-44, http://dx.doi.org/10.1080/00221687609499677.

[6] Abbott JE, Francis JRD. Saltation and suspension trajectories of solid grains in a water stream. Philos Trans R Soc London Ser A. 284 (1977) 225-54.

[7] Niño Y, García M, H. Experiments on saltation of sand in water. J Hydraul Eng. 124 (1998) 1014-25.

[8] Van Rijn LC. Sediment transport, part 1 : bed-Load transport. J Hydraul Eng. 110 (1984) 1431-56.

[9] Wiberg PL, Smith JD. A theoretical model for saltating grains in water. J Geophys Res. 90 (1985) 7341-54, http://dx.doi.org/10.1029/JC090iC04p07341.

[10] Cheng NS, Emadzadeh A. Average Velocity of Solitary Coarse Grain in Flows over Smooth and Rough Beds. J Hydraul Eng-ASCE. 140 (2014), http://dx.doi.org/10.1061/(asce)hy.1943-7900.0000875.

[11] Julien PY, Bounvilay B. Velocity of rolling bed load particles. J Hydraul Eng. 139 (2013) 177-86, http://dx.doi.org/10.1061/(asce)hy.1943-7900.0000657.

[12] Niño Y, García M, H. Gravel saltation 1. experiments. Water Resour Res. 30 (1994a) 1907-14.

[13] Lajeunesse E, Malverti L, Charru F. Bed load transport in turbulent flow at the grain scale: Experiments and modeling. J Geophys Res. 115 (2010) F04001, http://dx.doi.org/10.1029/2009jf001628.

[14] Houssais M, Lajeunesse E. Bedload transport of a bimodal sediment bed. J Geophys Res. 117 (2012) F04015, http://dx.doi.org/10.1029/2012jf002490.

[15] Papanicolaou AN, Diplas P, Balakrishnan M, Dancey C. Computer vision technique for tracking bed load movement. J Comput Civil Eng. 13 (1999) 71-9, http://dx.doi.org/10.1061/(Asce)0887-3801(1999)13:2(71).

[16] Furbish DJ, Haff PK, Roseberry JC, Schmeeckle MW. A probabilistic description of the bed load sediment flux: 1. Theory. J Geophys Res-Earth. 117 (2012) F03031, http://dx.doi.org/10.1029/2012jf002352.

[17] Tregnaghi M, Bottacin-Busolin A, Marion A, Tait S. Stochastic determination of entrainment risk in uniformly sized sediment beds at low transport stages: 1. Theory. J Geophys Res-Earth Surf. 117 (2012a) F04004, http://dx.doi.org/10.1029/2011jf002134.

[18] Valyrakis M, Diplas P, Dancey CL, Greer K, Celik AO. Role of instantaneous force magnitude and duration on particle entrainment. 115 (2010), http://dx.doi.org/10.1029/2008jf001247.

[19] Armanini A, Cavedon V, Righetti M. A probabilistic/deterministic approach for the prediction of the sediment transport rate. Adv Water Resour. 81 (2015) 10-8, http://dx.doi.org/10.1016/j.advwatres.2014.09.008.

[20] Ancey C, Heyman J. A microstructural approach to bed load transport: mean behaviour and fluctuations of particle transport rates. J Fluid Mech. 744 (2014) 129-68, http://dx.doi.org/10.1017/jfm.2014.74.

[21] Shim J, Duan J. Experiment study of bed load particle velocity. in: CL Patterson, SD Struck, DJ Murray, (Eds.). World Environmental and Water Resources Congress 2013 Environ. Water Resour. Inst. American Soc. Civil Eng., Cincinnati, OH, USA, 2013. pp. 1962-70.

[22] Shim J, Duan J. Experimental study of bed-load transport using particle motion tracking. Int J Sedi Res. under review (2015).

[23] Shim J, Duan JG. Stochastic properties of bed load transport. World Environmental and Water Resources Congress 2015 Environ. Water Resour. Inst. American Soc. Civil Eng.2015. pp. 1841-50.

[24] Duan J, He L, Wang GQ, Fu XD. Turbulent burst around experimental spur dike. Int J Sedi Res. 26 (2011) 471-523.

[25] Francis JRD. Experiments on the motion of solitary grains along the bed of a water-stream. Proc R Soc London Ser A. 332 (1973) 443-71.

[26] Lee HY, Chen YH, You JY, Lin YT. Investigations of continous bed load saltating process. 126 (2000) 691-700.

[27] Roseberry JC, Schmeeckle MW, Furbish DJ. A probabilistic description of the bed load sediment flux: 2. Particle activity and motions. J Geophys Res. 117 (2012) F03032, http://dx.doi.org/10.1029/2012jf002353.

[28] Shim J, Duan J. Experimental study of bed-load transport using particle motion tracking. In press (2016).

[29] Einstein HA. The bed load function for sediment transportation in open channel flows. 1950.

[30] Duan JG. Mean flow and turbulence around a laboratory spur dike. J Hydraul Eng. 135 (2009) 803-11, http://dx.doi.org/10.1061/(asce)hy.1943-7900.0000077.

[31] Cheng NS. Influence of shear stress fluctuation on bed particle mobility. Phys Fluids. 18 (2006), http://dx.doi.org/10.1063/1.2354434.

[32] Fredsøe J, Deigaard R. Mechanics of costal sediment transport. World Scientific, New Jersey, 1992.

[33] Cheng NS, Law AWK. Fluctuations of turbulent bed shear stress. J Eng Mech. 129 (2003) 126-30, http://dx.doi.org/10.1061/(asce)0733-9399(2003)129:1(126).

[34] Duan JG, Barkdoll BD. Surface-based fractional transport predictor: Deterministic or stochastic. J Hydraul Eng. 134 (2008) 350-3, http://dx.doi.org/10.1061/(asce)0733-9429(2008)134:3(350).

[35] Blinco PH, Simons DB. Characteristics of turbulent boundary shear-stress. J Eng Mech. 100 (1974) 203-20.

[36] Alfredsson PH, Johansson AV, Haritonidis JH, Eckelmann H. The fluctuating wall-shear stress and the velocity-field in the viscous sublayer. Phys Fluids. 31 (1988) 1026-33, http://dx.doi.org/10.1063/1.866783.

[37] Kimura M, Tung S, Lew J, Ho CM, Jiang F, Tai YC. Measurements of wall shear stress of a turbulent boundary layer using a micro-shear-stress imaging chip. Fluid Dyn Res. 24 (1999) 329-42, http://dx.doi.org/10.1016/s0169-5983(99)00002-7.

[38] Miyagi N, Kimura M, Shoji H, Saima A, Ho CM, Tung S, et al. Statistical analysis on wall shear stress of turbulent boundary layer in a channel flow using micro-shear stress imager. Int J Heat and Fluid Flow. 21 (2000) 576-81, http://dx.doi.org/10.1016/s0142-727x(00)00047-3.

[39] Buffington JM, Montgomery DR. A systematic analysis of eight decades of incipient motion studies, with special reference to gravel-bedded rivers. Water Resour Res. 33 (1997) 1993-2029, http://dx.doi.org/10.1029/96wr03190.

[40] Gail MH, Green SB. Critical values for the one-sided two-sample kolmogorov-smirnov statistic. J Amer Statist Assoc. 71 (1976) 757-60.

[41] Gleser LJ. Exact power of goodness-of-fit tests of kolmogorov type for discontinuous distributions. J Amer Statist Assoc. 80 (1985) 954-8.

[42] Young IT. Proof without prejudice - use of kolmogorov-smirnov test for analysis of histograms from flow systems and other sources J Histochem Cytochem. 25 (1977) 935-41.

Table 1. Flow parameter and sediment characteristics; uniform sediments with median size of 1.5 mm, and 2.4 mm; 26 experimental runs were performed

Case	D (m)	Q (m^3/s)	H (m)	S (m/m)	Re	Fr	u_* (m/s)	I_τ
1	0.0015	0.00072	1.1	0.031	4780	1.32	0.0537	0.51
2	0.0015	0.00072	1.1	0.035	4780	1.32	0.0574	0.51
3	0.0015	0.00104	1.4	0.021	6901	1.33	0.0493	0.40
4	0.0015	0.00115	1.5	0.023	7667	1.33	0.0528	0.37
5	0.0015	0.00127	1.6	0.016	8462	1.33	0.0451	0.35
6	0.0015	0.00193	2.1	0.016	12839	1.35	0.0504	0.26
7	0.0015	0.00207	2.2	0.016	13792	1.35	0.0513	0.25
8	0.0024	0.00072	1.1	0.024	4780	1.32	0.0480	0.51
9	0.0024	0.00072	1.1	0.035	4780	1.32	0.0574	0.51
10	0.0024	0.00093	1.3	0.023	6164	1.32	0.0497	0.43
11	0.0024	0.00127	1.6	0.021	8462	1.33	0.0521	0.35
12	0.0024	0.00140	1.7	0.010	9284	1.33	0.0378	0.33
13	0.0024	0.00152	1.8	0.021	10134	1.34	0.0547	0.31
14	0.0024	0.00165	1.9	0.017	11010	1.34	0.0510	0.29
15	0.0024	0.00179	2.0	0.020	11912	1.34	0.0559	0.28
16	0.0024	0.00179	2.0	0.021	11912	1.34	0.0571	0.28
17	0.0024	0.00193	1.8	0.010	10134	1.34	0.0531	0.31
18	0.0024	0.00193	2.1	0.017	12839	1.35	0.0531	0.26
19	0.0024	0.00207	2.2	0.016	13792	1.35	0.0513	0.25
20	0.0024	0.00207	2.2	0.017	13792	1.35	0.0541	0.25
21	0.0024	0.00222	2.3	0.021	14770	1.35	0.0602	0.24
22	0.0024	0.00252	2.5	0.017	16797	1.36	0.0568	0.22
23	0.0024	0.00268	2.6	0.019	17847	1.36	0.0576	0.21

Table 2. A summary of two sample K-S test results

Case	Static value $D_{m,n}$	Critical value $D_{m,n,\alpha}$	H_0
1	0.0534	0.1028	Do not reject
2	0.0531	0.1026	Do not reject
3	0.0605	0.1026	Do not reject
4	0.0547	0.1031	Do not reject
5	0.0844	0.1026	Do not reject
6	0.0617	0.1027	Do not reject
7	0.0802	0.1026	Do not reject
8	0.0702	0.1029	Do not reject
9	0.0723	0.1030	Do not reject
10	0.0679	0.1045	Do not reject
11	0.0693	0.1026	Do not reject
12	0.0536	0.1071	Do not reject
13	0.0613	0.1089	Do not reject
14	0.0657	0.1070	Do not reject
15	0.0584	0.1055	Do not reject
16	0.0602	0.1029	Do not reject
17	0.0883	0.1034	Do not reject
18	0.0857	0.1070	Do not reject
19	0.0881	0.1029	Do not reject
20	0.0626	0.1055	Do not reject
21	0.0652	0.1013	Do not reject
22	0.0960	0.1040	Do not reject
23	0.0697	0.1074	Do not reject

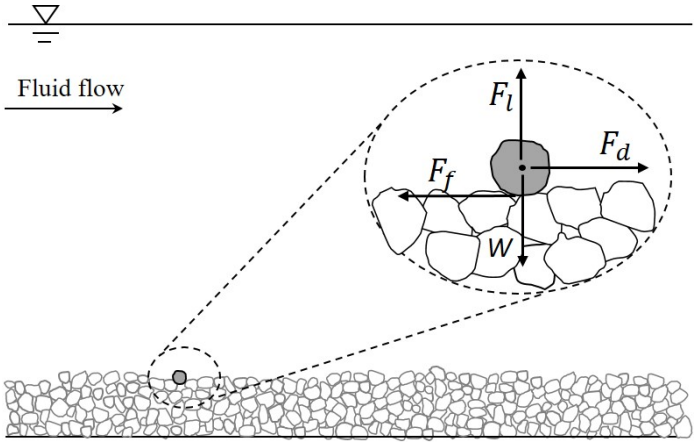

Fig. 14. Schematic sketch for moving particle

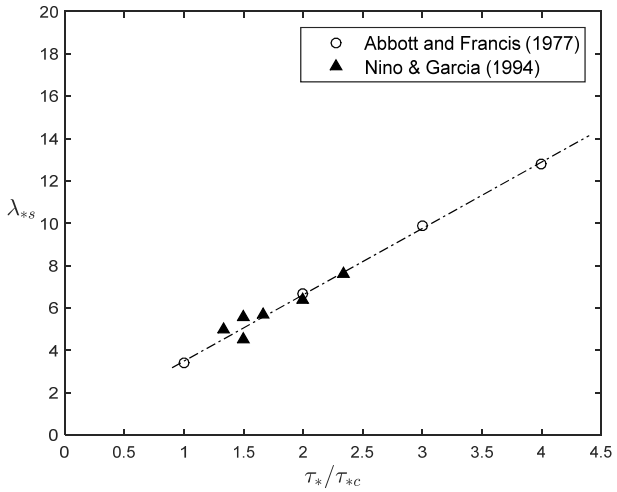

Fig. 15. Dimensionless of saltation length of sediment particle; The dimensionless saltation length (λ_{s*}) obtained from the experimental results of Abbott (1997) and Nino (1994)

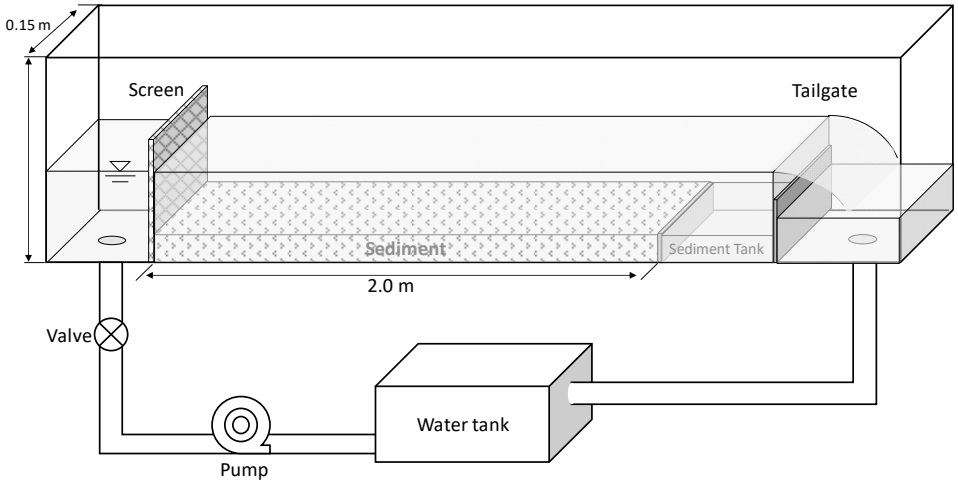

Fig. 3. Schematic of experimental setup

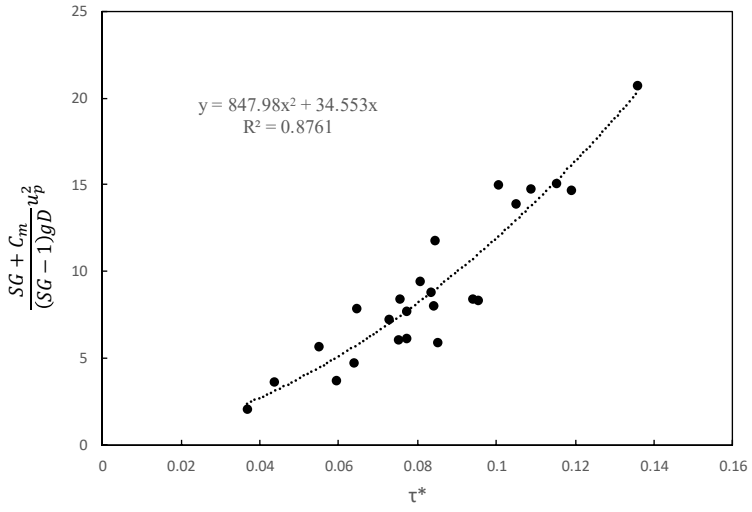

Fig. 16. The curve fitting of Eq. (22) using the experimental data

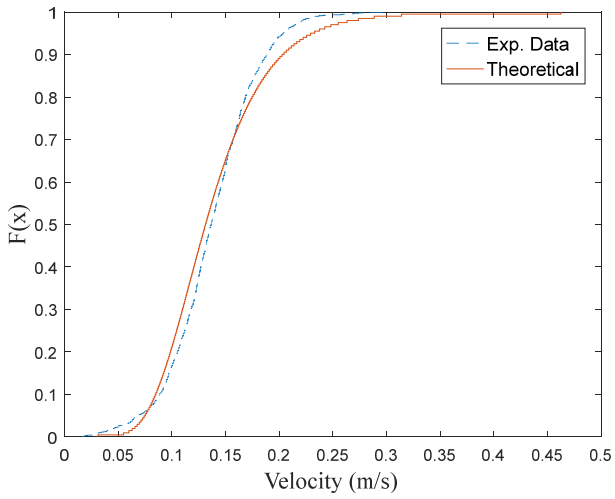

Fig. 17. K-S test of particle velocity distribution for Case 2 (u_*=0.0574). The x-axis is the particle velocity, and the y-axis is the cumulative probability. $D_{m,n} = 0.0828$ for this case.

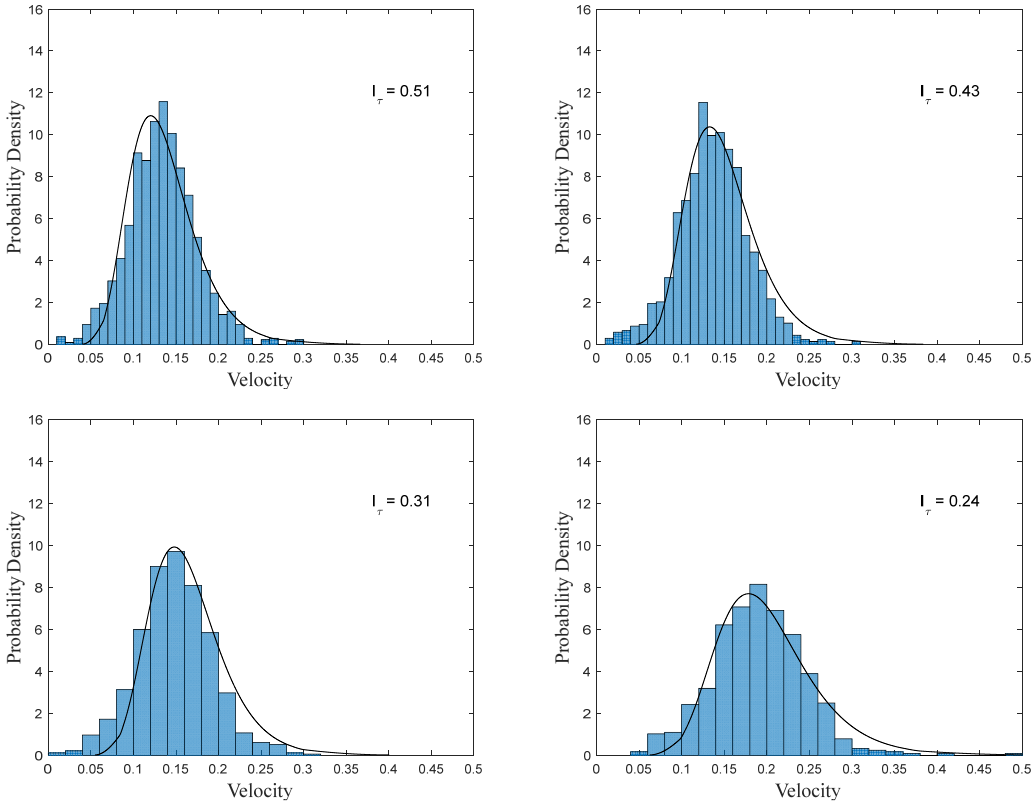

Fig. 6. Comparison of our model with experiment data for different intensity of bed-shear stress. The solid lines represent particle velocity distribution by using theoretical model. Columns are experiment data.

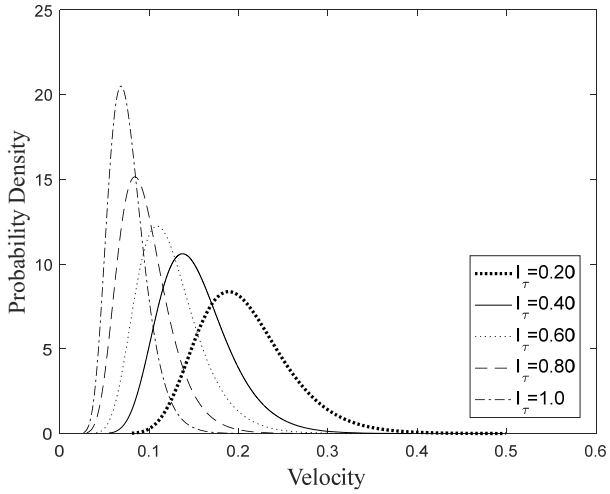

Fig. 7. The PDFs of particle velocity are computed using Eq. (13). with various I_τ , different PDFs of particle velocities are plotted.

APPENDIX C - SIMULATION OF DAM BREAK FLOW INDUCED SCOUR AROUND BRIDGE PIER USING SPH

Jaeho Shim[1], Jennifer Duan[2]

Department of Civil Engineering and Engineering Mechanics, University of Arizona, Tucson, AZ 85721, USA

Abstract

Bridge scour is commonly calculated based on the steady flow assumption. In practice, the peak discharge of a 100-year event is used for calculating the bridge scour depth. This will overestimate the scour depth, especially in arid and semi-arid regions where the typical storms are high-peak and short duration flash floods. This paper reports the experimental and numerical investigation of local scour around a bridge pier in dam break flow. A set of experiments were performed in a laboratory flume to produce dam break flow on a mobile bed with a pier installed at the downstream. Flow field, sediment particle velocity, and bed elevation changes were measured for each dam break experiment. These measurements were used to verify a numerical model of particle transport using the Smooth Particle Hydrodynamics (SPH) model. Experimental data first verified the model, and then was extended to a numerical flume to study bridge scour in high intensified dam break flow, which cannot be reproduced in the laboratory. The results showed the local scour depth is affected by the dam break flow which induced large sediment load. The peak scour depth was reached quickly, but only lasted for a few second before being back-filled by sediment. The ultimate scour depth is much smaller than the maximum scour depth.

Keywords: Bed load transport; particle tracking; particle velocity

1. Introduction

Scour is the primary cause of bridge failures in the United States. The Federal Highway Administration has estimated that over 60% of bridge failures were due to local scour. There are more than 20,000 bridges that are declared “scour critical” (Hunt 2009), and approximately 50 to 60 bridges fail each year in the United States (Brandimarte et al. 2012). Avoiding bridge failure caused by scour around piers is critical to human life and transportation infrastructure. Accurate estimation of the scour depth is important to prevent scour induced bridge failure. Therefore, the prediction of the local scour around piers is critical to bridge designs and public safety. Many experimental research studies have been used to develop expressions for the maximum scour depth at a bridge pier under clear water condition (Breusers et al. 1977; Raudkivi and Ettema 1983; Chiew and Melville 1987; Arneson et al. 2012). These relationships have been used extensively for engineering design.

Bridge scour is commonly calculated with the steady flow assumption. In practice, the peak discharge of a 100-year event is used for calculating the bridge scour depth. However, the general practice of employing peak-flow discharge to evaluate the maximum scour depth for design may be questioned because the maximum scour depth occurring under flash floods can be much smaller than the calculated value using peak-flow discharge, especially in arid and semi-arid regions where the typical storms are high-peak and short duration. In other words, using the peak-flow discharge for design can overestimate the maximum scour depth in comparison to the actual conditions under the flash flood or any unsteady hydrograph. Studies (Chang et al. 2004; Oliveto and Hager 2005) on unsteady floods have shown that the scour depth at bridge piers is usually smaller than that caused by a steady flow with the same peak discharges, unless the

duration of peak discharge is sufficiently long. Lu et al. (2008) performed field experiments to collect scour depth data during flood events. They compared the measured local scour depth with empirical formulas derived for the equilibrium scour depth for the peak flow discharges, and found that most of the formulas tend to overestimate the local scour depth. Therefore, when flow unsteadiness is pronounced, the temporal effect on scour depth should be considered. Kothyari et al. (1992) studied the temporal effects of unsteady flow on scour depth at bridge piers using a stepwise hydrograph. Chang et al. (2004) conducted an experimental study for bridge pier scour under steady and unsteady conditions by conducting stepwise hydrographs with different peak flow discharges and time to peaks. Oliveto and Hager (2005) experimentally investigated pier scour under flood waves, which are both single and double peak flow hydrographs. They proposed a computational procedure for the scour depth prediction. Hager and Unger (2010) investigated the scour depth due to a single-peak flood wave under clear water conditions, and proposed methods for the evolution of scour depth under unsteady flow. Lopez et al. (2014) performed experiments to investigate scour depth around piers under unsteady flood waves and presented an approach to estimate the final scour depth. Despite many research studies on local scour in a flood event, there are few investigations dealing with the movement of sediment particles under dam break flows in the local scour process.

This research aims to measure the velocity of sediment particles, and get an insight of scour hole forming processes around bridge piers. To get an insight of the scour process, scour monitoring is need for a better understanding of the local scour process and to enhance the numerical models' capability of scour simulation. Therefore, an experimental and numerical investigation of local scour around a bridge pier in dam break flow was conducted. A set of

experiments were performed in a laboratory flume to produce dam break flow on a mobile bed with a pier installed at the downstream. Flow field, sediment particle velocity, and bed elevation changes were measured in each dam break flow experiment. These measurements were used to verify a numerical model of particle transport using the Smooth Particle Hydrodynamics (SPH) model. The model was first verified with experimental data, and then was used as a numerical flume to study bridge scour in highly intensified dam break flow, which cannot be reproduced in the laboratory.

2. Numerical Model

2.1 Smoothed Particle Hydrodynamics (SPH) method

The prediction of local scour can be achieved by three-dimensional (3D) flow and sediment transport model. Traditional computational fluid dynamics (CFD) techniques (e.g. volume-of-fluid methods (VOF)) have been used to study wave structure interactions (Kleefsman et al. 2005) and to design breakwaters (Higuera et al. 2013). However, Eulerian numerical methods, such as the ones based on finite volume method, require expensive mesh generation and have severe technical challenges associated with implementing conservative multi-phase schemes that can capture the nonlinearities within rapidly changing geometries. Thus, the emergence of meshless schemes has provided a much needed alternative, the mesh free method.

In the past two decades, the Lagrangian approach, Smoothed Particle Hydrodynamics (SPH) (Gingold and Monaghan 1977), has emerged as a meshless method. SPH is a fully Lagrangian meshless method, where the material to be simulated is represented as discrete particles which move according to the governing dynamics. The method is meshless, and

requires no special treatment of free surface, therefore avoiding costly mesh generation. Therefore, the Lagrangian method of SPH is the ideal method for large nonlinear deformation flows. The scheme has been applied to a variety of problems such as free-surface flows (Gomez-Gesteira et al. 2010), flood simulations (Vacondio et al. 2012), coastal flows (Dalrymple and Rogers 2006), and geotechnical problems (Bui et al. 2007). Also, Gomez-Gesteira and Dalrymple (2004) used SPH to study the classical dam-break problem in three dimensions. Within the field of coastal engineering, Gotoh et al. (2004) studied the wave-breakwater interaction, and Khayyer and Gotoh (2009) used it to predict wave impact pressure due to sloshing waves. This method uses particles to represent fluid, and these particles' motion was governed by the dynamic principles. When simulating free-surface flow, the Lagrangian method of SPH allows the domain to be multiply-connected without a special treatment of free surface (Violeau 2012).

Adequately resolving the interface is essential to capture complex flows accurately with variable physical properties for each phase, such as free surface flows around bridge piers. Hence, a multi-phase SPH simulation requires a huge number of particles and a small time step, which means many iterations in a given simulation period. Therefore, despite its suitability for such problems, SPH is well known for being an expensive method computationally (Crespo et al. 2011), and multi-phase SPH simulations actually involve many more particles that further increase the computational demands and costs (Mokos et al. 2015). In recent years, the massively parallel architecture of graphic processing units (GPUs) has emerged as a viable option to process a large number of particles. The parallelization on GPUs makes them suitable for SPH (Herault et al. 2010; Crespo et al. 2011). In this study, a GPU is chosen to accelerate SPH

simulation. Herein, we used the open source DualSPHysics code (Crespo et al. 2015) to include the two-phase liquid-solid model. DualSPHysics is a CPU/GPU solver package with pre- and post-processing tools capable of performing simulations on millions of particles using the GPU architecture targeted to practical engineering problems involving nonlinear, fragmented, and free-surface flows.

2.2 Governing equation of the SPH method

The basic principle of the SPH formulation is the integral representation of the function *f(x), which* represents a numerical or physical variable defined over a domain of interest Ω at a point *x*. The integral approximation or kernel approximation according to Gingold and Monaghan (1977):

$$f(x) \approx \int_{\Omega} f(x')W(x-x',h)dx' \tag{1}$$

with *h* defined as the smoothing length that characterizes the size of the support domain of the kernel and *W* the weighting or kernel function. The kernel function is chosen to be a smooth, isotropic and even function with compact support. A fifth-order Wendland kernel is used as a weight function. In a discrete domain Eq (1) can be approximated by using an SPH summation in the form of

$$\langle f(x)\rangle = \sum_{j}^{N} f(x_j)W(x-x_j,h)V_j \tag{2}$$

where V is the volume of the particle expressed as the ratio of the mass *m* to density ρ and N is the number of particles within the support. By simplifying the approximation parentheses and the order of approximation term, the final form of the particle approximation in discrete form is

$$f(x)=\sum_{j}^{N}\frac{m_j}{\rho_j}f_j W_{ij} \tag{3}$$

with $W_{ij}=W(x_i-x_j,h)$ and $f_i=f(x_j)$. In the SPH model, the computation domain is discretized into a set of particles, which possess material properties, such as mass, velocity, density and pressure. Under the framework of the large eddy simulation, the mass and momentum equations of particles are derived from the Navier-Stokes equations by using a spatial filter and written as follow:

$$\frac{D\rho}{Dt}=-\rho\nabla u \tag{4}$$

$$\frac{Du}{Dt}=\frac{\nabla P}{\rho}+g+\nu_0\nabla^2 u+\frac{1}{\rho}\nabla\tau \tag{5}$$

where t is time, ρ is fluid density, u is particle velocity, P is pressure, g is the gravity, ν_0 is the laminar kinematic viscosity, and the τ is shear stress, which is approximated by the sub-particle scale (SPS) model as follows

$$\tau_{m,n}=\rho\nu_t\left(\frac{\partial u_m}{\partial x_n}+\frac{\partial u_n}{\partial x_m}-\frac{2}{3}\delta_{m,n}\sum\nolimits_{k=1}^{3}\frac{\partial u_k}{\partial x_k}\right)-\frac{2}{3}\rho C_1\Delta^2\delta_{m,n}\|S\|^2 \tag{6}$$

where the constant parameter C_1=0.0066, Δ is the initial particle spacing, $\delta_{m,n}$ is the Kronecker delta, and the shear stress component directions m and n follow the Einstein notation. The turbulent viscosity is determined by the Smagorinsky turbulent model ($\nu_t=(C_{smag}\Delta)^2\|S\|$), where C_{smag} is the Smagorinsky constant. The strain rate tensor is $S_{m,n}=0.5(\partial u_m/\partial x_n+\partial u_n/\partial x_m)$ and its norm is defined by $\|S\|=\sqrt{2S_{m,n}S_{m,n}}$, which is further expanded as

$$\|S\|^2 = 2\sum_{m=1}^{3}\left(\frac{\partial u_m}{\partial x_m}\right)^2 + \sum_{m=1,n>m}^{3}\left(\frac{\partial u_m}{\partial x_n} + \frac{\partial u_n}{\partial x_m}\right)^2 \quad (7)$$

In terms of numerical parameters, the sub-particle scale (SPS) viscosity model, with the Smagorinsky constant of 0.2 is used.

3. Laboratory Experiment and Numerical Setup

3.1 Experiment setup

The experiments for this study were performed in a 0.45 m wide, 2.7 m long flume filled with a layer of sediment on the bed. Flow discharge was controlled by a water tank installed at the front of the flume. At the beginning of each experiment, the tank is filled up with water, and a 1 cm thick plate gate is erected to separate the downstream section and the water tank. The dam break flow was generated by suddenly lifting the gate. A circular pier was placed 1.4 m from the gate. Figure 1 is the schematic experimental setup, which shows the location of the test section and the camera. The particle motion was measured from the side. A Sony commercial camera, Model XCD-V60, was installed on the side of the test section. It is capable of taking images at a resolution of 640×480 pixels with a rate of up to 90 fps. In each run, over 1,300 consecutive images were taken at 90 fps in about 16 seconds. The channel's bed was filled with approximately 7 cm thick of sediment. A uniformly sized sediment of d_{50} = 2.4 mm, with a density of ρ_s = 2,650 kg/m^3, was used. A particle tracking algorithm was developed to track particle trajectory (Shim and Duan 2016) using the motion detection algorithm in OpenCV Library (http://code.opencv.org). This image processing technique is capable of accurately

detecting all the moving particles so that their instantaneous velocities can be calculated by comparing two consecutive images.

3.2 Numerical model setup

A three-dimensional hydrodynamic model is required to examine the fluid field around the bridge pier and the role of sediment transport in the scour process. The multi-phase model in DualSPHysics code is applied to simulate the bam break flow induced scour around the bridge pier. In DualSPHysics, the experimental domain is discretized into a collection of particles with a particle size of 0.004 m. The numerical simulation is performed in a rectangular box 2.0 m long, 0.45 m wide and 0.60 m high surrounding the pier. The length of the numerical flume was reduced to minimize the number of SPH particles, this allowed a reduction in the simulation time. But, the circular pier was placed at the same location 1.4 m from the gate as the physical model. The peak flow from dam break is controlled by the total volume of water in the tank. The maximum water depth in the tank is 1 m, and the tank is 0.3 m long, 0.45 m wide. As a result, the total number of particles needed is about 1.2 million, of which 0.6 million are fluid particles, and 0.4 million are sediment particles. The remaining particles are boundary and gate particles. To ensure that the free surface is smooth and physically acceptable, the particle density is Shephard filtered every 20 steps (Dalrymple and Rogers 2006). Regarding the speed of sound C_s, it is chosen based on the principle that the ratio C_s/u_{max} should be larger than 10 (Monaghan 1994). The numerical simulations were carried out by running DualSPHysics on NVIDIA GeForce 950 GPUs. The numerical model simulated 3 seconds of the physical experiment, and it requires approximately 40 *Hrs* of computation for cases with a bridge pier downstream.

4. Experimental Observation and Simulation Results

4.1 Model validation

In order to verify the SPH model, the simulated results of particle velocities around the bridge pier were compared with laboratory measurements. Using the image analysis technique, all the moving particles around the pier in the dam break flow were detected, and their instantaneous velocities were obtained. The numerical results were visualized through an open source tool called the *Paraview,* and the particle velocities from the numerical experiment were collected by the *Paraview* tool (Fig 2). This software can distinguish multiple moving particles and track the motion of particles around pier.

A validation of DualSPHysics using this dam break test case are shown in Fig. 3 where the probability density of measured instantaneous particle velocity were compared with numerical experimental data. In the numerical experiment, 21,890 instantaneous particle velocities around the bridge pier were collected. The probability density of experimental instantaneous particle velocity around the bridge pier were in good agreement with the numerical value. Particle velocities from the numerical simulation are higher than the experimental data for $V < 0.18$ m/s. And, most of particle velocities for $V > 0.18$ m/s are similar with the experimental data.

4.2 Bed surface elevation

The test case of dam break flow induced scour around the bridge pier at 0.2 sec are shown in Fig. 4. The gate is located at 30cm from the flume entrance. A total of 3 numerical cases were simulated in three different test conditions by varying initial water depth in the tank for h=30, 50,

100 cm. The dam break flow was generated by lifting the 1cm thick gate. Fig. 5 shows several significant image frames concerning the scour process around the pier which occurred during one of the numerical runs carried out with reference to the initial condition of water tank height (h=30cm, 50 cm). After the gate opens, in test case h=30cm, the dam break flow freely spreads over the sediment bed and reaches the front of the pier around at t= 0.6 sec, whereas the test case h=50cm shows the flow wave arrives around t=0.49sec. By comparing the bed surface evolution at the front of the pier in different flow conditions, it is clearly seen that there is a strong influence of water volume on the scour depth. Also, comparisons of bed surface elevations between the test cases for h=30cm and h=50cm are shown in Fig. 6. The results of instantaneous bed surface profile at t=2 sec along the cross section at 1.35 m (in front of pier) and 1.4 m (in the middle of pier) are shown in Fig.6. The x axis shows the transverse coordinate at the measurement section, the t coordinate indicates the elapsed time starting from the time of gate lifting, and the z coordinate shows the bed surface elevation. It is seen that the scour depth in front of the pier reaches the maximum after 0.2 seconds of the wave arrival, and then gradually decreases due to back-filled by sediment. However, the difference of maximum scour depth between these two test cases are very small. This perhaps is attributed to the water volume in the tank not being different enough to see its influence on scour depth.

Therefore, the largest possible flow volume was experimented by filling up the tank to 100 cm water depth. Comparison of bed surface profiles along the channel centerline at different times is shown in Fig. 7 and Fig. 8 for test cases, h=50 cm and h=100cm, respectively. In the case, h=100cm, the maximum scour depth is approximately 30 mm, which is about 10 times deeper than the one in the test case h=50cm. Fig. 9 shows the time series of flow rate at six

different points along the centerline of the channel. In this figure, the peak flow rate at 1.37 m (in front of bridge pier) occurred at 0.6 seconds after the gate was opened, which is the same time at which the maximum scour depot occurs. It is seen that the scour depth increases during the rising limb of flow hydrograph, and when the flow rate starts to decrease, scour depth decreases rapidly due to sediment back-fill (see Fig. 8 and Fig. 9). The results indicate that the scour depth increases significantly as the flow rate increases, and the maximum scour depth is not only affected by the peak flow rate but also the time to peak.

4.3 Maximum scour depth evolution

Finally, the maximum scour depth calculated using HEC-18 recommend equations was compared with the simulated maximum scour depth for test case h=100cm. The pier scour equation recommended by the Federal Highway Administration in HEC-18 is called CSU equation. It is based on laboratory data and applicable for both live-bed and clear water scour, given as (Richards et al. 1990)

$$\frac{d_s}{b} = 2.0 K_s K_\theta K_b K_a \left(\frac{y_1}{b}\right)^{0.35} F_1^{0.43} \tag{8}$$

in which d_s= maximum scour depth, b = the pier width, K_s = pier shape factor (1.0 for circular cylinder), K_θ = pier skewness factor (1.0 for θ=0), K_b= correction factor for bed condition (1.1 for clear-water scour and 1.1 for live-bed scour), K_a= bed armoring factor (1.0 for sand bed material), y_1= flow depth directly upstream of the pier, and F_1= approach flow Froude number= $V_1/(gy_1)^{1/2}$, V_1= mean velocity of flow directly upstream of the pier (m/s) and g = acceleration of gravity (m/s^2). Also, Jain (1981) proposed a formula for maximum clear-water scour around cylindrical pier, it is given by

$$\frac{d_s}{b} = 1.35\left[\frac{y_1}{b}\right]^{0.3} \quad (9)$$

The simulated maximum scour depth is compared with the calculated results using these two equations (Eq. 8 and Eq. 9), in which the peak flow is used. The results are shown in Table 1. It is seen that maximum scour depth occurring under the unsteady flow is much smaller than the calculated value using the peak-flow discharge. In other words, using the peak-flow discharge for calculating scour depth will overestimate it. Therefore, when flow unsteadiness is pronounced, the temporal effect on scour depth should be considered. The actual scour depth is much smaller than the scour depth calculated by using the peak flow in HEC-18 equations.

5. Conclusion

The numerical simulation of sediment transport around a bridge pier was conducted by using the Smooth Particle Hydrodynamics (SPH) model. The results from the DualSPHysics SPH model showed the scour process around bridge pier in dam break flow is affected by the total flow volume from the dam break flow. To calibrate and verify the model, the modelling results of particle velocities were comparted with laboratory experimental results at the same condition. And then used as a numerical flume to study bridge scour in highly intensified dam break flow, which cannot be reproduced in the laboratory. The results showed the local scour depth is affected by the dam break flow induced large sediment load. The peak scour depth was reached quickly, but only lasted for a few seconds before being back-filled by sediment. The ultimate scour depth is much smaller than the maximum scour depth. At present, the simulation domain is small, and the water tank volume is limited, due to the large number of particles needed for the SPH model. Therefore, further research on the parallel computing method to speedup simulation

is needed to extend the simulation to field cases.

References

Arneson, L. A., Zevenbergen, L. W., Lagasse, P. F., and Clopper, P. E. (2012). "Evaluating Scour at Bridges." 5th, ed., U.S. Department of Transportation, 340.

Brandimarte, L., Paron, P., and Di Baldassarre, G. (2012). "Bridge pier scour: a review of processes, measurements and estimates." 11(5), 975-989.

Breusers, H. N. C., Nicollet, G., and Shen, H. W. (1977). "Local scour around cylindrical piers." 15(3), 211-252.

Bui, H. H., Sako, K., and Fukagawa, R. (2007). "Numerical simulation of soil-water interaction using smoothed particle hydrodynamics (SPH) method." 44(5), 339-346.

Chang, W. Y., Lai, J. S., and Yen, C. L. (2004). "Evolution of scour depth at circular bridge piers." 130(9), 905-913.

Chiew, Y. M., and Melville, B. W. (1987). "Local scour around bridge piers." 25(1), 15-26.

Crespo, A. C., Dominguez, J. M., Barreiro, A., Gomez-Gesteira, M., and Rogers, B. D. (2011). "GPUs, a New Tool of Acceleration in CFD: Efficiency and Reliability on Smoothed Particle Hydrodynamics Methods." 6(6).

Crespo, A. J. C., Dominguez, J. M., Rogers, B. D., Gomez-Gesteira, M., Longshaw, S., Canelas, R., Vacondio, R., Barreiro, A., and Garcia-Feal, O. (2015). "DualSPHysics: Open-source parallel CFD solver based on Smoothed Particle Hydrodynamics (SPH)." 187, 204-216.

Dalrymple, R. A., and Rogers, B. D. (2006). "Numerical modeling of water waves with the SPH method." 53(2-3), 141-147.

Gingold, R. A., and Monaghan, J. J. (1977). "Smoothed particle hydrodynamics- theory and application to non-spherical stars." 181(2), 375-389.

Gomez-Gesteira, M., and Dalrymple, R. A. (2004). "Using a three-dimensional smoothed particle hydrodynamics method for wave impact on a tall structure." 130(2), 63-69.

Gomez-Gesteira, M., Rogers, B. D., Dalrymple, R. A., and Crespo, A. J. C. (2010). "State-of-the-art of classical SPH for free-surface flows." 48, 6-27.

Gotoh, H., Shao, S. D., and Memita, T. (2004). "SPH-LES model for numerical investigation of wave interaction with partially immersed breakwater." 46(1), 39-63.

Hager, W. H., and Unger, J. (2010). "Bridge Pier Scour under Flood Waves." 136(10), 842-847.

Herault, A., Bilotta, G., and Dalrymple, R. A. (2010). "SPH on GPU with CUDA." 48, 74-79.

Higuera, P., Lara, J. L., and Losada, I. J. (2013). "Simulating coastal engineering processes with OpenFOAM (R)." 71, 119-134.

Hunt, D. (2009). *Monitoring scour critical bridges*, Transportation Research Board, Washington, D.C.

Jain, S. C. (1981). "Maximum clear-water scour around circular piers." 107(5), 611-626.

Khayyer, A., and Gotoh, H. (2009). "Wave Impact Pressure Calculations by Improved SPH Methods." 19(4), 300-307.

Kleefsman, K. M. T., Fekken, G., Veldman, A. E. P., Iwanowski, B., and Buchner, B. (2005). "A Volume-of-Fluid based simulation method for wave impact problems." 206(1), 363-393.

Kothyari, U. C., Garde, R. C. J., and Raju, K. G. R. (1992). "Temporal variation of scour around circular bridge piers." 118(8), 1091-1106.

Lopez, G., Teixeira, L., Ortega-Sanchez, M., and Simarro, G. (2014). "Estimating Final Scour Depth under Clear-Water Flood Waves." 140(3), 328-332.

Lu, J. Y., Hong, J. H., Su, C. C., Wang, C. Y., and Lai, J. S. (2008). "Field measurements and simulation of bridge scour depth variations during floods." 134(6), 810-821.

Mokos, A., Rogers, B. D., Stansby, P. K., and Dominguez, J. M. (2015). "Multi-phase SPH modelling of violent hydrodynamics on GPUs." 196, 304-316.

Monaghan, J. J. (1994). "Simulating free-surface flows with sph." 110(2), 399-406.

Oliveto, G., and Hager, W. H. (2005). "Further results to time-dependent local scour at bridge elements." 131(2), 97-105.

Raudkivi, A. J., and Ettema, R. (1983). "Clear-water scour at cylinderical piers." 109(3), 338-350.

Richards, E. V., Simons, D. B., and Julien, P. Y. (1990). "Highways in the River Environments." Federal Highway Adminstration, U.S Department of Transportation, Washington D. C., FHWA-HI90-016.

Shim, J., and Duan, J. (2016). "Experimental study of bed-load transport using particle motion tracking." In press.

Vacondio, R., Rogers, B. D., Stansby, P. K., and Mignosa, P. (2012). "SPH Modeling of Shallow Flow with Open Boundaries for Practical Flood Simulation." 138(6), 530-541.

Violeau, D. (2012). Fluid Mechanics and the SPH Method. Oxford University Press, Oxford, Oxford University Press, Oxford.

Table 1 Comparison of maximum scour depth (d_s)

	d_s *(cm)*
Richardson et al., (1990)	7.02
Jain (1981)	7.60
Simulated Depth	3.80

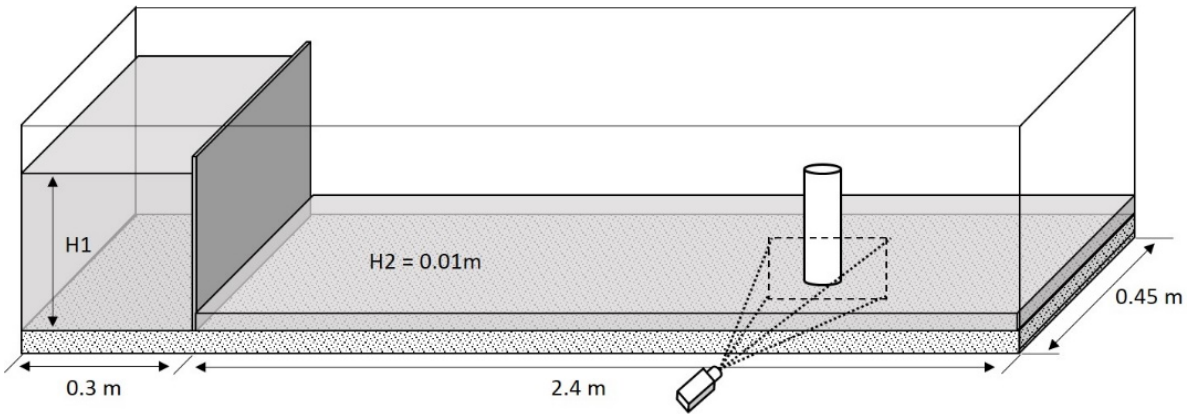

Figure 1 Schematic of experimental setup

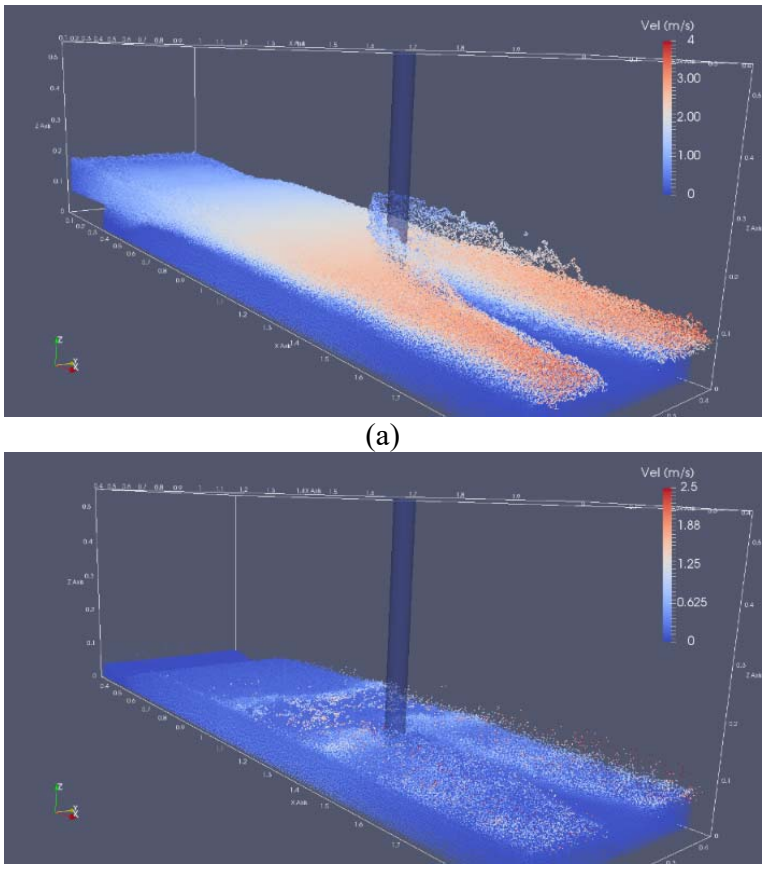

Figure 2 Visualization of Dam break flow impacting on pier, (a): liquid –sediment phase, (b): sediment phase

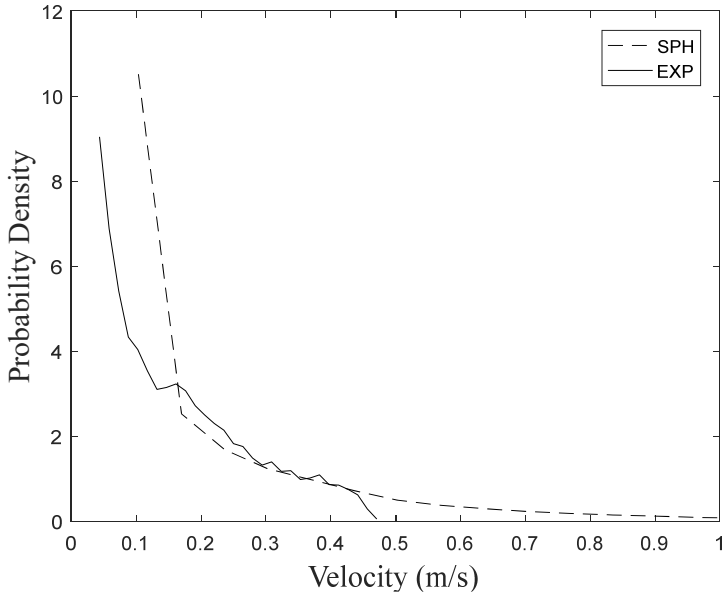

Figure 3 Probability density of instantaneous velocity

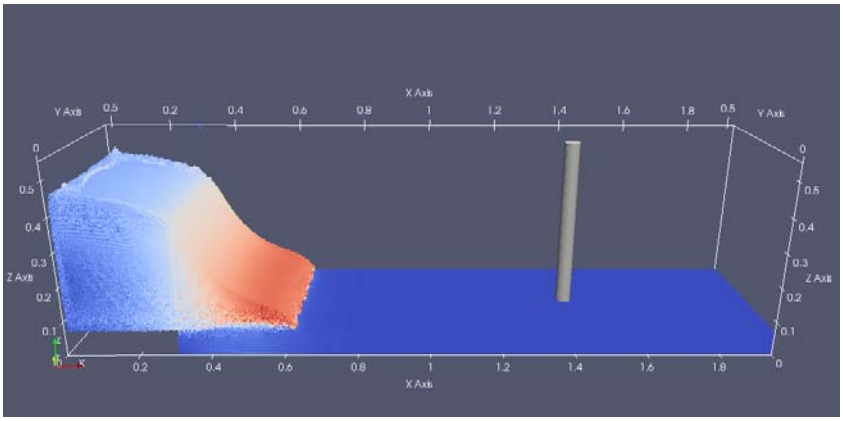

Figure 4 Dam break flow at t=0.2sec, and h=50cm

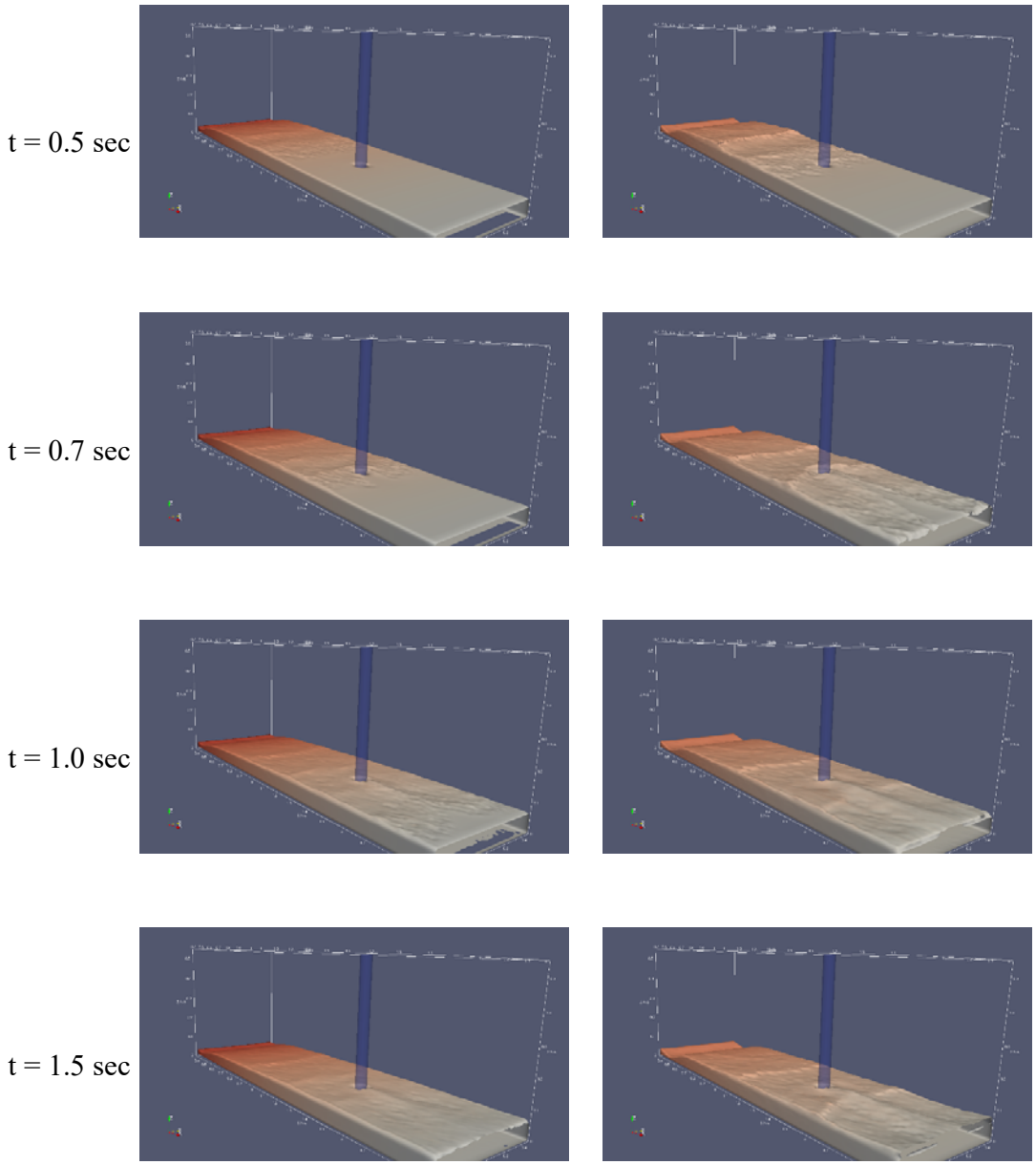

Figure 5 Dam break flow impacting on pier (sediment phase), Case 1 (left column): tank height is 30 cm , and Case 2(right column): tank height is 50 cm.

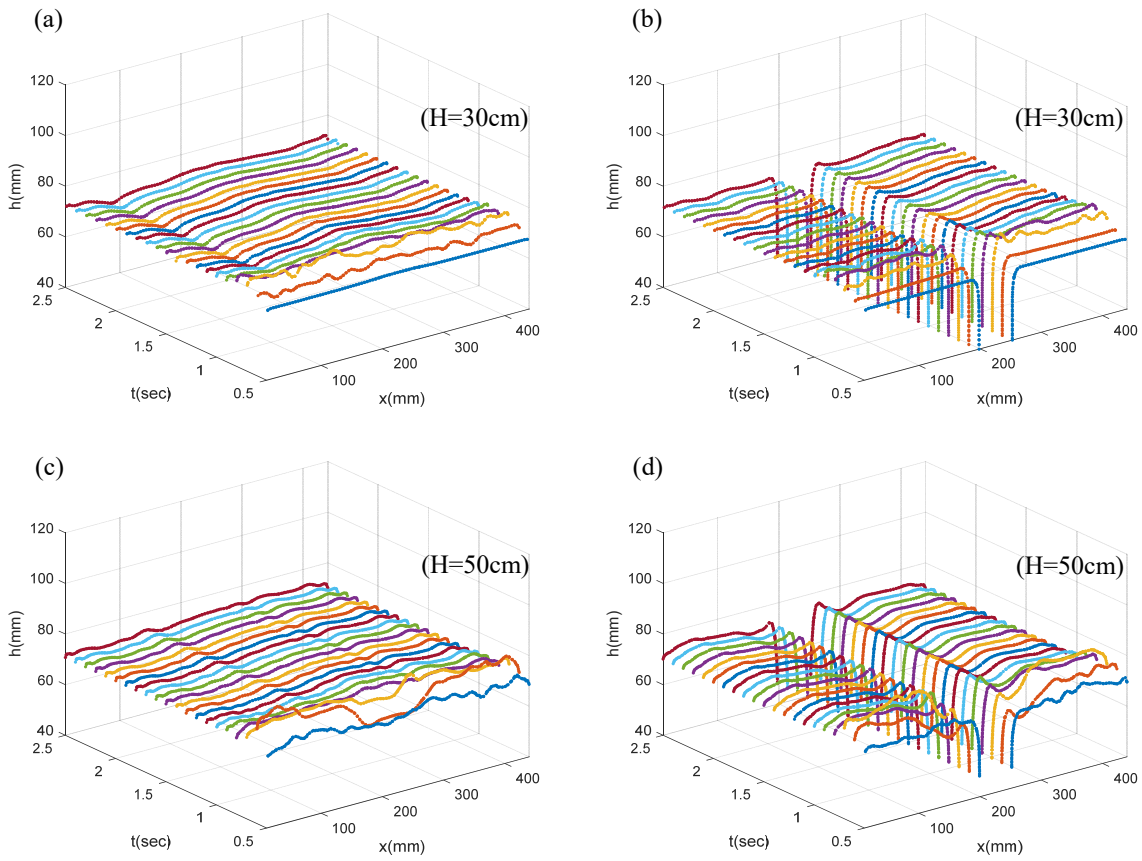

Figure 6 Comparison of bed surface profiles in front of bridge pier (left column), in the middle of bridge pier (right column). Initial depth of water tank h=30 cm (a, b) and h=50 cm (c, d)

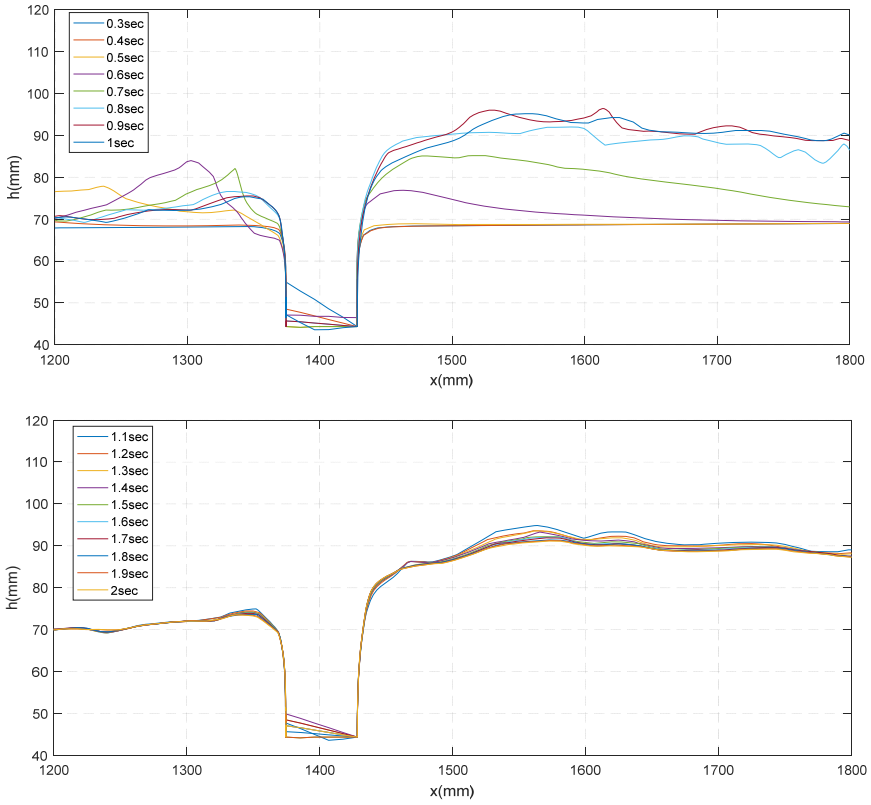

Figure 7 Streamwise bed surface elevation profile along the centerline of channel , h=50cm

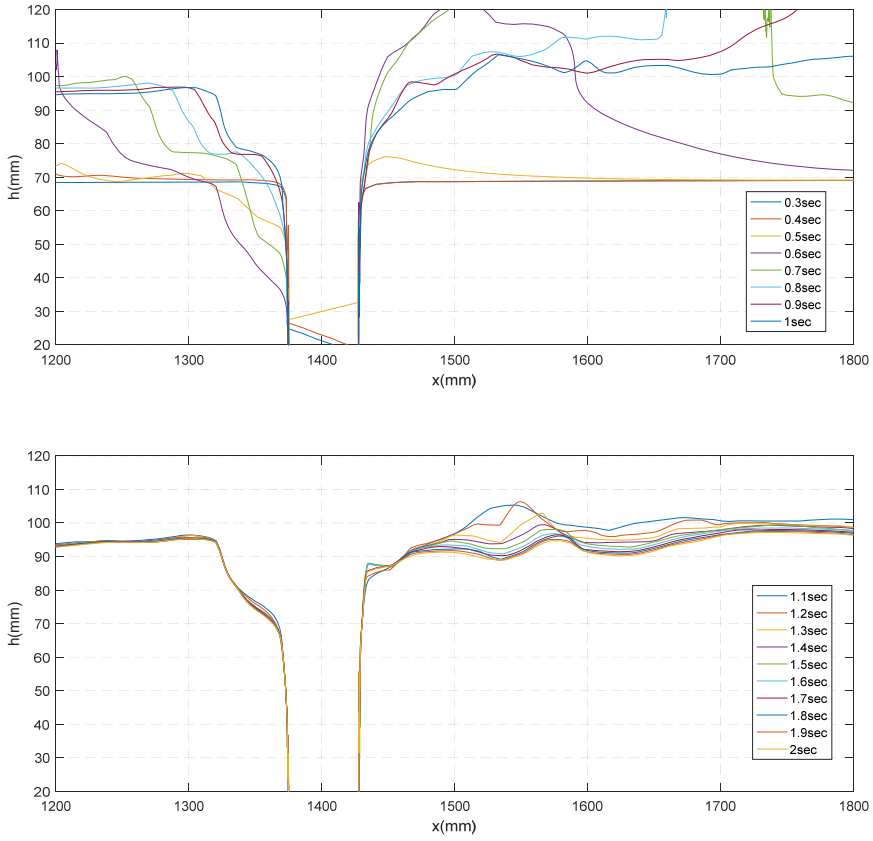

Figure 8 Streamwise bed surface elevation profile along the centerline of channel, h=100cm (extreme condition)

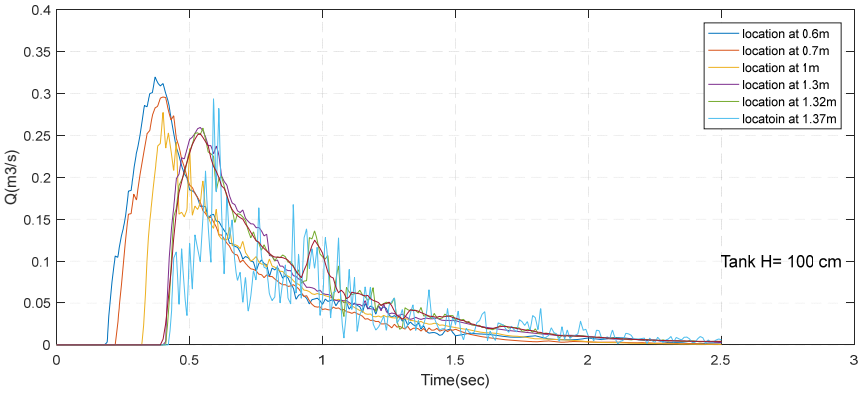

Figure 9 the time series of the flow rate at six different point along the centerline of the channel